Energy 223 (2021) 120037

Contents lists available at ScienceDirect

Energy

journal homepage: www.elsevier.com/locate/energy

Investigation on a full-scale heat pipe heat exchanger in the ceramics industry for waste heat recovery

Hussam Jouhara [a, *], Delpech Bertrand [a], Brian Axcell [a], Luca Montorsi [b], Matteo Venturelli [b], Sulaiman Almahmoud [c], Massimo Milani [a], Lujean Ahmad [a], Amisha Chauhan [a]

[a] Heat Pipe and Thermal Management Research Group, College of Engineering, Design and Physical Sciences, Brunel University London, UB8 3PH, UK
[b] University of Modena and Reggio Emilia, Department of Science and Methods for Engineering, 42122, Reggio Emilia, Italy
[c] Spirax Sarco Engineering PLC, Cheltenham, GL51 9NQ, UK

ARTICLE INFO

Article history:
Received 25 November 2020
Received in revised form
10 January 2021
Accepted 31 January 2021
Available online 11 February 2021

Keywords:
Heat pipe heat exchanger
Heat pipes
Waste heat recovery
Ceramic industry
Computational fluid dynamics

ABSTRACT

The ceramics industry is the second largest energy consuming sector in Europe. The main energy used in the ceramics industry is heat generated through burners using natural gas. The main area can be identified in three stages, the drying stage and the firing stage, and the cooling stage. The firing stage represents about 75% of the total energy cost. The roller hearth kiln technology is considered to be the most cost-effective solution for ceramic tile manufacturing. The kiln is separated into two sections, the firing stage and the cooling stage. The cooling stage generates large amounts of waste heat as the exhaust of the kiln is composed of a challenging flue gas for heat recovery. The recovery of this heat in an efficient way with no cross contamination has been achieved with a heat pipe heat exchanger (HPHE) system, which was designed, manufactured and installed on a roller hearth kiln and is presented in this paper. The heat pipe heat exchanger located next to the cooling section exhaust stack managed to recover up to 100 kW at steady state without cross contamination or excess fouling. The return on investment of the system has been evaluated at 16 months with a saving of £30,000 per year. This paper will present a deep row by row theoretical analysis of the heat pipe heat exchanger. The Computational Fluids Dynamics will also be presented to investigate the fluid dynamics within the evaporator and condenser section. Both investigations have then been validated by the experimental investigation carried out on a full-scale industrial system. The design approach used in this paper will highlight the benefits of this type of technology and provide a guideline for the design of novel heat pipe heat exchangers.

1. Introduction

Four types of production can be identified in the traditional ceramics sector: tiles, tableware, sanitary ware and brick and heavy clay pipe. Most of the manufacturing companies are based in Italy, Spain and Poland. The tile manufacturing sector groups all the items used for covering roofs, floors, walls, showers, and other objects such as furniture for bathroom and kitchen. The tile ceramic industry is the largest sector within the traditional ceramics sector. Tile manufacture represents a market of 14 billion Euros and 75% of the total energy consumption regarding the other traditional ceramics sector. Ceramic tiles consume large amounts of natural gas and the emissions related to the natural gas consumption are evaluated at about 265 kg of CO_2 per tonne of fired tile. The energy used in the manufacturing of tiles is around 28 kWh/m^2 [1]. The main challenges of the ceramic tile industry are the competition for mass volumes of tiles fired at low prices with a good product quality to compete with emerging economies, the high energy demands of the tile manufacturing process and the reduction of greenhouse gas emissions. To overcome those challenges, the ceramic tile sector needs to develop new ways of reducing the consumption of energy (in the roller kiln, 50% of the total energy consumption is used for the firing). The increase in production required to compete with emerging economies comes with issues such as defects that will affect the production quality. Technologies needs to be developed to reduce those defects. The EU legislation regarding greenhouse gas emissions imply a reduction of the

* Corresponding author.
E-mail address: Hussam.Jouhara@brunel.ac.uk (H. Jouhara).

https://doi.org/10.1016/j.energy.2021.120037

Nomenclature

Symbols Unit

A	Surface area (m^2)
A_{1e}	Bare area for the heat pipe in the Evaporator (m^2)
A_{1c}	Bare area for the heat pipe in the Condenser (m^2)
A_{2e}	Fins area for the heat pipe in the Evaporator (m^2)
A_{2c}	Fins area for the heat pipe in the Condenser (m^2)
C	Heat capacity rate ($W.K^{-1}$)
Cst	cost (£/year)
C_P	Specific heat ($J.kg^{-1}.K^{-1}$)
C_r	Heat capacity ratio, ($C_r = C_{min}/C_{max}$) dimensionless
C_{sf}	Constant in *Rohsenow* correlation depending on the surface-fluid combination dimensionless
D	Diameter (m)
E	Energy (kWh)
g	Gravitational acceleration ($m.s^{-2}$)
h	Heat transfer coefficient ($W.m^{-2}.K^{-1}$)
h_{fg}	Latent heat of vaporization ($J.kg^{-1}$)
k	Thermal conductivity of the heat pipe wall ($W.m^{-1}.K^{-1}$)
K_e	Equivalent heat transfer coefficient accounts for the contribution of the pipe walls and of the Evaporation ($W.m^{-2}.K^{-1}$)
K_c	Equivalent heat transfer coefficient that accounts for the contribution of the pipes' walls and of the Condensation ($W.m^{-2}.K^{-1}$)
L	Length (m)
$\dot{m}$	Mass flow rate ($kg.s^{-1}$)
n_{total}	Number of pipes
Nu	Nusselt number, ($Nu = hD/k$) dimensionless
P_{fin}	Fin pitch m
Pr	Prandtl number, ($Pr = \mu c_p/k$) dimensionless
Q	Heat transfer rate (W)
R	Thermal resistance ($°C.W^{-1}$)
R_{time}	Working hours (hr)
Re	Reynolds number, ($Re = \rho VD/\mu$) dimensionless
S_L	Longitudinal pitch of the staggered arrangement (m)
S_L	Transverse pitch of the staggered arrangement (m)
T	Temperature ($°C{\cdot}K^{-1}$)
U	Overall heat transfer coefficient ($W.m^{-2}.K^{-1}$)
V	Velocity ($m.s^{-1}$)

Greek Symbols

Δ	Difference
ε	Effectiveness dimensionless
η	Efficiency dimensionless
ρ	Density ($kg.m^{-3}$.)
σ	Surface tension ($N.m^{-1}$)
μ	Dynamic viscosity (Pa.s)
χ^*	Ratio of pipe pitch to pipe diameter dimensionless

Subscripts

c	Refers to Condenser section
ci	Internal surface of the condenser
co	External surface of the condenser
$cond$	conduction
e	Refers to Evaporator section
ei	Internal surface of the evaporator
eo	External surface of the evaporator
f	fin
h	Heat
hp	Heat Pipe
$HPHE$	Heat Pipe Heat Exchanger
l	liquid
L	Longitudinal
LM	Logarithmic
max	Maximum
NG	Natural gas
o	outer
out	outlet
s	Wall surface
sat	saturation
T	Transverse
v	Vapour

emissions in the tile manufacturing process. By reducing the energy consumption, the emissions will also reduce. In ceramics manufacturing, some gaseous pollutants are produced, such as SO_X, NO_X, HF, and HCL. Reducing the emissions of these gases will be achieved by developing new filter technology and reducing the energy consumption.

The tiles can be identified in 3 groups:

- Roof tiles used to protect buildings against the rain; they can be made of terracotta or slate but also concrete and plastic, in particular applications.
- Floor and wall tiles are used to cover interior surface for decorative purposes.
- Ceiling tiles are used inside buildings for decoration, but also to improve the acoustics.

The manufacturing process of the tiles depends on the type of tiles produced. In this paper the process investigated is based on the roller hearth kiln technology. The tile can be unglazed, single glazed or double glazed. Five main steps can be identified in the process: the raw material and body preparation, the shaping, the drying, the firing and the final product shipping. A schematic representing the manufacturing process of tiles can be seen in Fig. 1.

The preparation of the tile body is one of the most crucial stages in the manufacturing process. The composition of the tile needs to be carefully selected in order to produce a high-quality tile meeting the mechanical and visual requirements. The tile is composed of a combination of natural and synthetic materials such as aluminium silicate-based clay and small amounts of pigment, metal oxides or colorants. The prepared raw material is mixed in a controlled environment using water as a bonding agent (around 35%). Then, the preparation is dried using spray drying at temperature between 350 °C and 450 °C to a water content of 5%–9%. The resulting product is a powder with a moisture content of 5%. The shaping can be done using impact toggle presses, screw presses or hydraulic presses with a pressure of about 35 MPa. The tile is then dried. The dryer technology depends on the production; tunnel dryers, roller dryers or vertical dryers are used. The drying is performed at a temperature which depends on the dryer technology used (200–220 °C for vertical dryers, 300–350 °C for tunnel dryers). The tiles are dried for between one and 4 h depending on the moisture content. The moisture content at the end of the drying stage cannot exceed one percent to avoid fissure or explosion of the material during the firing stage. The heat required for the dryers is supplied via waste heat from the kiln or by combustion of natural gas. The main issue with the waste heat recovered from the kiln is the

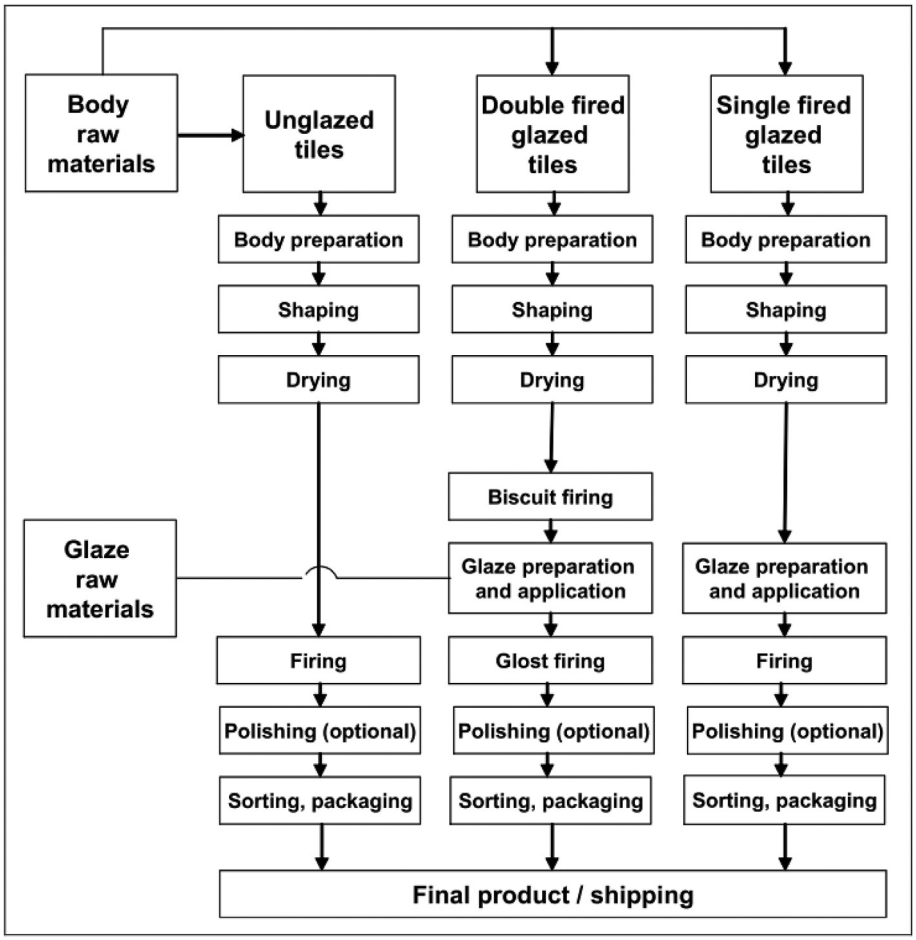

Fig. 1. *Schematic of the tiles manufacturing process* [2].

composition of the exhaust gas, which will affect the quality of the final product. The main purpose of the firing stage is to bind molecules of the tile together to increase the mechanical properties and guarantee a good integrity of the tiles. The firing process depends on the technology used. Two main kiln technologies can be used in the ceramics process, the tunnel kiln and the roller hearth kiln. Nowadays the most commonly used technology in tile manufacturing is the roller hearth kiln but some technologies used in tunnel kilns can be applied in roller hearth kilns with regard to the waste heat recovery of exhaust stack gases. Four stages can be identified in the firing process: the firing stage, where the tile is heated up to 1300 °C, direct cooling using an air stream on the tile (1300 °C–700 °C), indirect cooling using radiative cooling (700 °C–300 °C), and the slow cooling using air to cool down the tile to 30 °C. A cross section of the firing kiln can be seen in Fig. 2.

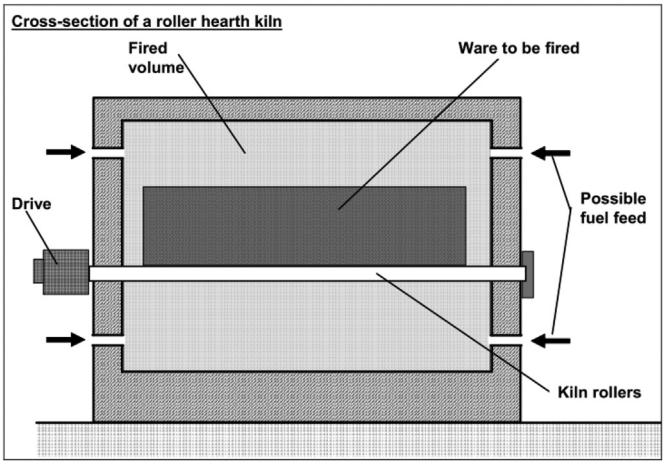

Fig. 2. Cross-section of a roller hearth kiln [3].

2. State of the art

2.1. Ceramics industry

Waste heat recovery has been widely investigated due to global warming and climate change. Indeed, companies and governments are trying to reduce greenhouse emissions and waste energy, for example, the United State of America wasted 57% of the energy produced in 2008 [4]. To prevent such issues, universities and companies have developed technology to recover the heat from high or low-grade temperatures. Those actions can prevent global warming but also can reduce manufacturing and energy costs. The main areas of energy consumption during the manufacture of tiles are the firing, accounting for 50% of total energy consumption, the spray drying (36%), and the drying (9%) [1]. Also, the CO_2 emissions of the firing process are estimated to be about 265 kg CO_2/t of fired tile [5]. High energy demanding processes need to decrease energy consumption in order to remain competitive and to lower the

production cost [6]. To match this objective, energy saving technologies have been investigated in the ceramic tile industry.

Several optimisations have been tested and applied in the drying stage, such as [7]:

- Optimization of the recirculation of drying air: using more sophisticated ventilation techniques to control fundamental parameters such as relative humidity, temperature and flow rate improved the efficiency of the hot-air dryer.
- Waste heat recovery: clean hot air from the cooling exhaust of the firing kilns is available and can significantly improve the efficiency of the process. Waste heat recovery can provide up to 100% of potential energy saving for the drying process.
- Pulsed hot air: a periodically interrupted flow allows the use of higher drying air temperatures; this solution allows enough time for the moisture to migrate from the centroid to the surface. These higher air temperatures allow a reduction in the drying time of 40 min when compared with the process with a classical roller dryer.
- Microwave drying: microwave assisted drying has two obvious advantages. First of all, only the object is heated, whilst the chamber remains cool, and so the energy to heat the drying chamber is saved. The microwave also heats the centre of the body and not only the surface; this promotes moisture migration to the surface. Water absorbs the microwave better than the raw materials, which considerably accelerates the drying. The use of microwave technology can significantly reduce the drying time (from 7 to 30 min, depending on the object/material), with a higher energy efficiency [8].

A significant number of investigations have been conducted regarding waste heat recovery from the kiln cooling stage. The application of the Organic Rankine Cycle (ORC) for the ceramic industry has been investigate by B. Peris et al. [9]. The ORC has proved its efficiency for waste heat recovery from low-grade heat sources. Similar to the Rankine cycle, the operative principle consists of recovering the waste thermal energy from a heat source via a working fluid to an expander in order to produce mechanical work which is subsequently converted to electricity. The heat is taken from exhaust gases from a ceramic furnace via a collector heat exchanger to the ORC. A simulation of the ORC system has been conducted for a typical year of production. The final results showed an energy production for the whole year in excess of 115 MWh. This ORC could save around 237 MWh of primary energy and avoid about 31 tonnes per year of atmospheric CO_2 emissions [9]. The payback period of applying the ORC was around 4–5 years [9]. Hot air from the cooling zones of tunnel kilns is usually used in the drying stage and added to the hot air from gas burners. This method of recovering hot air can be managed only if the length of the pipes (distance between the cooling and the drying zone) is limited. A significant amount of insulation is needed over the pipe section to limit thermal losses. A large amount of energy is saved using this technique of heat recovery. Some processes also use a heat exchanger to recover the heat from the cooling zone to preheat the combustion air and the air for the drying stage. The application is limited due to the production of acidic combustion gases and other phenomena such as foaming. Some applications use a thermal oil as a working fluid to transfer the recovered heat to the drying and firing stages [2,10]. Cogeneration systems can be applied in the ceramic sector due to the simultaneous need of heat and electricity. Cogeneration technology has been applied in the ceramic industry to recover the waste heat from the cooling stage [2]. The hot air from the drying stage is used in the dryer and in the cogeneration system via a heat exchanger placed in the kiln cooling zone. Fresh air from the factory is injected into the system. The fresh air is mixed with the hot air coming from the cooling stage and the hot air coming from the cogeneration system and other gas engine emissions from the factory. Then, the hot air is sent in the dryer and a gas burner maintains the desired heat in the dryer. If the hot air temperature is too high, the uncooled gases from engines are withdrawn immediately. With this process, 10%–50% of the heat input can be saved [11,12].

2.2. Heat pipe technology

Heat pipe are considered as one of the most efficient and passive ways to transfer the heat from a hot source to a heat sink. A heat pipe is a sealed shell composed of three sections, an evaporator, an adiabatic section, and a condenser. The evaporator section is where the heat is input into the heat pipe. The working fluid at the evaporator boils and changes phase into saturated vapour. This saturated vapour travels upwards through the adiabatic section to the condenser section. The working fluid vapour condenses and releases the latent heat to the heat sink, then, the working fluid liquid flows back to the evaporator. The cycle is then repeated as presented in Fig. 3. The heat pipe system has multiple benefits such as an isothermal surface which eliminates any hot or cold spots, which will increase the lifetime of the system for applications where the exhaust is corrosive. The heat pipe is considered as a passive device. No pumping/mechanical components are needed to move the liquid working fluid back to the evaporator. The reaction time of heat pipes is higher than for other heat transfer systems, which offers different control options. Due to their advantages, such as an isothermal surface, high thermal conductivity and the independency of each heat pipe in the system, the heat pipe heat exchanger (HPHE) technology is a good candidate for most of the corrosive, high fouling and high temperature exhaust applications. Heat pipe systems are composed of different shapes and technologies to move the fluid in the tubes. Heat pipes can use two methods to move the fluid and the vapour between the condenser

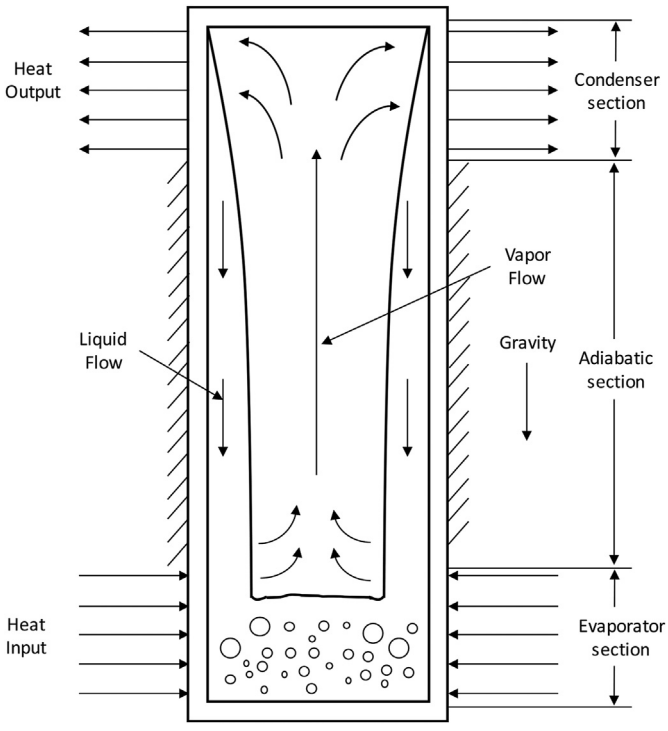

Fig. 3. Operation cycle of a gravity assisted heat pipe.

and the evaporator. Gravity can be used to return the fluid from the condenser, this method is the easiest and cheapest option. The second way is to use a wick structure in the inner wall of the heat pipe. This method allows the possibility of having the evaporator section above the condenser section. Heat pipes rely on the two-phase heat transfer to transfer the heat from the evaporator section to the condenser section. The return of the liquid in wickless heat pipes (thermosyphons) relies only on gravity without the need for a wick structure. Thus, the manufacture of gravity-assisted heat pipes is simpler and cheaper than for other technologies. Thermosyphons can operate using different working fluids such as water, refrigerants, liquid metals, or organic oils such as Dowtherm.

The effects of the selection of working fluid on heat pipe performance was investigated by *Jouhara* et al. [13]. Two fluids types were investigated. Water, FC-84, FC-77 and FC-3283 were tested in a 200 mm long pipe with an inner diameter of 6 mm. The evaporator and condenser lengths were respectively 40 mm and 60 mm. The results highlighted the capacity, at higher heat fluxes, of water as a working fluid. At low heat fluxes, the FV-84 outperformed the water, this is due to a lower boiling point compared to the other working fluids. Thermosyphons have also been investigated using R134a and R404a by *Fadhl* et al. [14] using CFD modelling of the two-phase phenomena. The aim was to investigate the behaviour and CFD of low temperature boiling point fluids for transferring heat in an efficient way. It was highlighted that the refrigerant was able to transfer heat at low temperatures and the CFD model developed was in good accordance with the experimental results. The use of thermosyphons to transfer heat from a heat source to a heat sink have been widely investigated in different industrial and commercial applications. Heat pipe applications in industrial setups vary from ceramics to metals and pharmaceuticals. Heat pipe technology can address a variety of problems because of its advantages. The isothermal nature of the heat pipe was utilised for cooling PV cells uniformly, as demonstrated by *Jouhara* et al. [15]. The heat pipe arranged on the flat surface can maintain the temperature of the PV for the optimal electrical output. A similar heat pipe arrangement was used by *Jouhara* et al. [16] to maintain a suitable temperature for the battery pack of a car. As the temperature of the battery increases, the battery can become unstable. To prevent the failure of the battery pack, the charging and discharging times are increased, thus decreasing the temperature but reducing the efficiency of the battery. By installing a flat heat pipe on the bottom of the battery, the authors managed to maintain a low battery temperature in fast charge and discharge regimes.

When installed in tube bundles, the heat pipes may be considered as a heat pipe heat exchanger. The heat pipes will then be able to transfer heat from a heat source, i.e. flue gas or waste heat, to a cold clean stream with no cross contamination and low maintenance. HPHEs have been applied in a variety of applications. The heat pipes are placed in a shell and attached to a plate in a staggered arrangement. As the heat pipe provide a uniform temperature. Due to the two-phase heat transfer occurring in the heat pipe shell, the temperature of the outer wall is uniform. This feature of the heat pipe allows a better control of the suspension of particles and will reduce the fouling which occurs in shell and tube heat exchangers. As the heat pipes are placed on a separation plate, the cross contamination will be close to none. In contrast, shell and tube heat exchangers are challenging to maintain as the shell does not have any inspection door, the shell needs to be cut and re-welded to clean the flue gas side. Heat pipe heat exchangers, due to their geometry, are much easier to maintain as inspection doors can easily be installed.

HPHEs are a suitable solution for recovering heat in many industrial applications as outlined by *Egilegor* et al. [17] in the ETEKINA project, which aims to utilise heat pipe heat exchangers in three industries, namely, aluminium, steel and ceramics. The aim of the project is to recover 40% of waste heat in exhaust streams. The expected output of this project is to annually recover up to 597 MWh, 3020 MWh and 4003 MWh, in each respective industry, with a significant reduction in CO_2 emissions. The scale of the heat pipe heat exchangers being developed in the Etekina project are larger than the one presented in this paper. The design of HPHE is a complex process to achieve. Issues such as heat pipe temperature and the system footprint can be challenging. In this regard, *Brough* et al. [18] conducted an experimental and computational study on a vertical multi-pass heat pipe heat exchanger. The system was connected to a ceramic kiln to recover heat at a temperature of 270 °C and it managed to recover up to 63 kW. To improve the replicability and versatility of the application, a TRNSYS model was developed. *Brough* et al. [18], also performed a TRNSYS model based on the system presented in this paper. The prediction model shown a recovery of about 65 kW for similar exhaust temperature. The difference in the thermal performance is due to various reasons such as the number of heat pipes, hot and cold stream flow rates, and the logarithmic mean temperature difference. The TRNSYS model predicted the experimental value within ±15%. *Lukitobudi* et al. [19] investigated the use of HPHEs using water as a working fluid to recover heat in industry with medium temperature ranges, below 300 °C. The heat pipes were composed of plate finned copper tubes staggered in the heat pipe heat exchanger shell. The heat source used for the test was an electrical heating element. The finned heat pipe heat exchanger was able to recover more heat than similar heat exchanger systems. In the high temperature range, the heat pipe was determined to not be safe as the pressure in the heat pipe could exceed the maximum pressure allowed. The use of copper as a heat pipe shell presents the advantage of decreasing the conduction resistance at the cost of a lower maximum allowed pressure. The use of stainless steel or carbon steel heat pipes for heat pipe heat exchangers at higher temperatures is recommended. A commercial application of this system was also discussed by the author and the annual predicted waste heat recovery under the test conditions was determined to be 314 GJ/yr. *Yang* et al. [20] used a water-steel heat pipe heat exchanger to recover heat from a bus exhaust. Nine heat pipes were staggered in the heat exchanger casing. A test rig was then developed and tested at three inlet temperatures, 100 °C, 200 °C and 300 °C. The heat transferred by the heat pipes to the heat sink was respectively 1989 W, 3550 W and 6490 W. The heat pipe heat exchanger was able to recover heat using a compact arrangement for mobile vehicle applications. *Ramos* et al. [21] investigated the use of a crossflow heat pipe based heat exchanger to recover waste heat. A numerical model was built to predict the heat recovered by the heat pipe-based heat exchanger and compared with experimental results. The developed

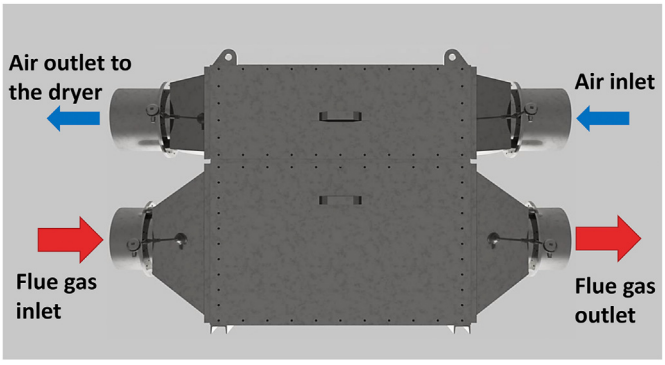

Fig. 4. HPHE system.

model validated for several flow rates and temperature points was on average predicting the temperatures of the heat pipe with a 5% error in the evaporator and 7% in the condenser section. *Jouhara* et al. [22] investigated a novel heat pipe based heat exchanger to recover waste heat from data centres. The system installed in the air conditioning unit was able to increase the efficiency of the air conditioning for a payback of less than a year. *Almahmoud* et al. [23] examined a novel flat heat pipe system using parallel tubes connected with a bottom collector and a condenser top header. The system was exposed to a high temperature heat source. The heat recovered by radiation was transferred to a water coolant via the shell and tube condenser section. Different experimental setups were used with different heat source temperatures and a prediction model was developed. The accuracy of the theoretical model could predict the heat pipe performance within 25% error. Similarly, a radiative heat pipe ceiling was developed by *Delpech* et al. [24] to recover heat by radiation from ceramic tiles. The heat pipe was composed of a horizontal evaporator connected to a condenser section located outside the kiln. The system was tested in the laboratory and confirmed the use of horizontal heat pipe evaporator sections for recovering heat from a radiative heat source.

2.3. CFD modelling

Numerical simulation tools are gaining an important role in the design process of complex systems and have demonstrated good reliability for the investigation of the intricate phenomena that characterise these systems [25]. In addition, the design of complex systems can be improved by adopting a numerical approach for the evaluation and testing of different solutions and configurations. Furthermore, numerical analysis enables the study of system performance under time dependent operating conditions. In the literature, many examples can be found of the use of numerical tools for the simulation of energy systems in general. Regarding the ceramic industry, in Ref. [26] a combined numerical approach has been developed in order to investigate the energy efficiency improvement of a ceramic kiln by means of the exhaust gases recovery from a CHP turbine unit. An additional study related to the ceramic sector can be found in Ref. [27]: a 0D/1D model has been used to investigate the thermal fluid dynamic behaviour of a ceramic roller kiln and a mechanical stress analysis has been performed to evaluate the final residual stresses in the product. In a similar way, a thermal and structural numerical analysis has been used in Ref. [28] to analyse the evolution of the temperature distribution and the thermo-mechanical stresses due to liquid aluminium injection through a nozzle. Bhutta et al. [25] presented a review that focuses on the application of computational fluid dynamic (CFD) analysis in the field of heat exchangers. They identified that the CFD technique represents a valid alternative for the design and optimization of heat exchangers since the numerical results are in good agreement with experimental data to within 2%–10%. In Ref. [29] a CFD analysis has been used for the investigation of the effect of inlet air flow maldistribution on the thermo-hydraulic performance of heat exchangers. In 2016, Pal et al. [30] investigated the heat transfer and flow distribution for different configurations of heat exchanger with and without baffles and highlighted the importance of computational fluid dynamics for gaining the optimum design. In Ref. [31] a CFD simulation and a multi-objective optimization were integrated to enhance the performance of a heat exchanger. In 2016, Ramos et al. [32] conducted an experimental and analytical analysis on an air-to-water heat exchanger finding a good agreement between the experimental and numerical results in terms of outlet temperature, i.e. a difference of 3% in the evaporator and a difference of 5% in the condenser. Danielewicz et al. [33] studied the heat losses from the pre-insulated pipes of a district heating network, performing CFD simulations on a real underground application.

In [34], a combined numerical approach has been used to determine the performance of a heat recovery system for the post-combustion flue gas treatment in a coffee roaster plant. In this study, the optimization of the design of the shell and tube heat exchanger has been obtained with a CFD approach.

In this paper, the CFD simulation of the full geometry of the convective heat pipe heat exchanger is carried out considering the material thermal properties and the working parameters of the heat pipes. The influence of the fins of the heat pipes on the heat recovery are considered in the calculation. The performance of the system is investigated under actual operating conditions with a steady-state simulation. The simulation provides the thermal behaviour of the system in terms of temperature, pressure and velocity distribution; moreover, the heat transfer recovered in the evaporator and in the condenser is determined. The numerical results are validated by correlating the numerical temperatures of the outlets and the thermal power recovered by both the streams to the experimental measurements. Delpech et al. [35] investigated numerically the impact of utilising heat pipe technology for waste heat recovery from a ceramic kiln exhaust. The numerical model of the kiln presented energy savings by the HPHE of 863 MWh per annum. In this study, the HPHE thermal performance is investigated theoretically and numerically using mathematical and CFD models and validated experimentally.

Table 1
Design temperatures for the evaporator and condenser sections.

Air mass flow rate flue gas	6000 kg/h
Air mass flow rate condenser	2640 kg/h
Flue gas inlet temperature	204 °C
Flue gas outlet temperature	145 °C
Air inlet temperature	30 °C
Air outlet temperature	164 °C

Fig. 5. HPHE on the platform.

2.4. Heat pipe heat exchanger novelty

The HPHE unit presented in this paper was applied to a ceramics roller hearth kiln under the scope of the Horizon 2020 project, Dream, which investigated the use of novel and innovative technologies to reduce energy consumption within the ceramics

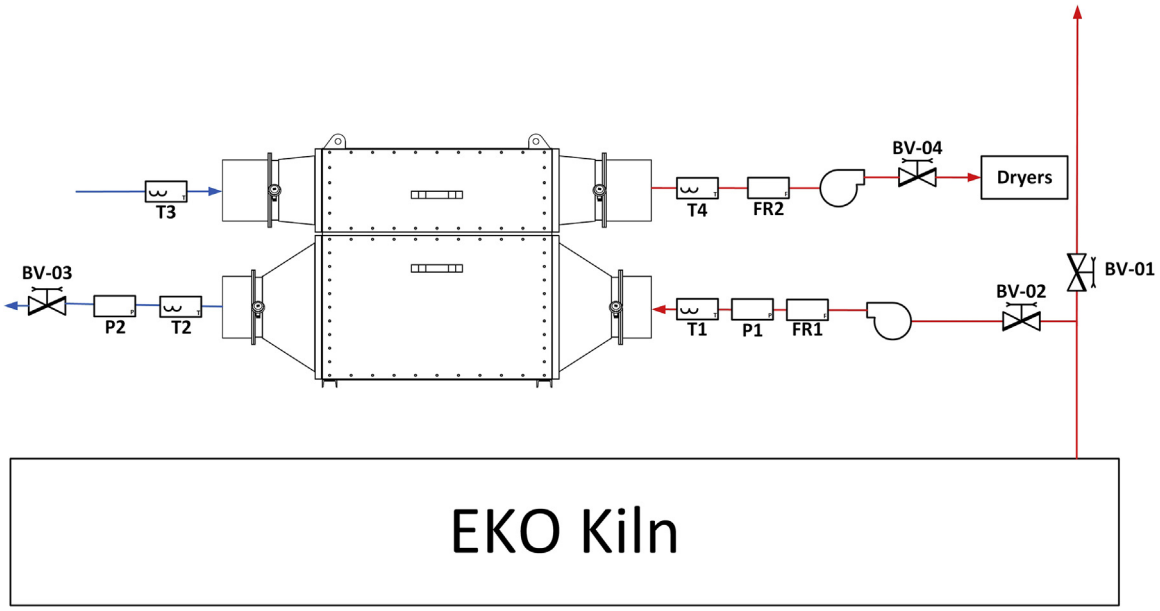

Fig. 6. HPHE P&ID system.

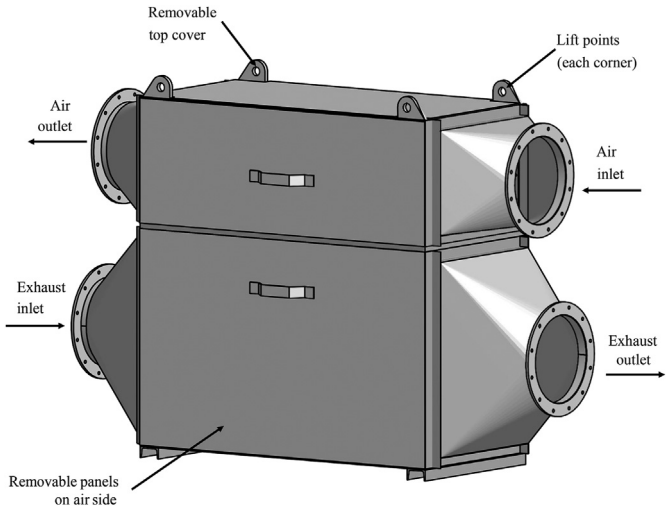

Fig. 7. Isometric view HPHE.

industry. Every HPHE unit has a bespoke design due to the distinctive requirements of the end user and, as such, all HPHEs are tailor made. The HPHE presented in this paper is a cross flow, finned, HPHE that will be fully independent and invisible to the process operation. This type of HPHE has not been applied yet to the ceramics sector. Also, the use of this configuration has not been investigated before for this application. In this paper, the theoretical design of the heat pipe is presented in depth with a row-by-row analysis of the system. Also, a deep investigation of the flow in both the evaporator and condenser sections was carried out using Computational Fluid Dynamics software. This allows replicability and validation of the theoretical model using both simulation and experimental investigations.

3. Methodology

3.1. Experimental apparatus

The HPHE was composed of 180 helical finned heat pipes arranged in 18 rows. The diameter of each heat pipe was 38 mm, and the total length was 1.5 m. Each heat pipes were finned to enhance the heat transfer rate. The fins were 1 mm thick at a height of 10 mm with a pitch of 4 mm. The heat pipe shell was made of carbon steel with water as a working fluid. As shown on Fig. 4, the heat pipe system consists of a condenser section and an evaporator section. The flue gas goes through the evaporator section at the bottom of the heat pipe heat exchanger. The heat is then transferred to the condenser through the heat pipes. Then air is forced through the condenser section. In order to design the system, the flue gas had to be characterized. The flue gas temperature and the composition has been recorded using a flue gas analyser, flow meter and temperature probe (see Table 1). The HPHE has been designed according to these results for an average heat recovery of 100 kW.

The heat pipe heat exchanger has been installed on a platform located next to the kiln exhaust. A photo of the installed system can be seen in Fig. 5. The dimensions and features of the heat pipe heat exchanger can be found in Fig. 7 and Fig. 8. The system has been instrumented with K-type thermocouples on the inlet and outlet of the evaporator section (T1-T2) and on the condenser section (T3-T4). The thermocouples were connected to a National Instruments data logger using NI PXIe-4353. Pressure sensors (Omega PX1009) have also been installed on the exhaust streams to monitor the pressure drop of the system due to the finned design (see Fig. 6). Pitot probes were installed in the flue gas and the air stream. The flow rate in the condenser and evaporator section was controlled with two fans to maintain a steady temperature for the outlet temperature of the condenser section, thus protecting the heat pipes from overheating. All the results were stored in a data logger installed on site.

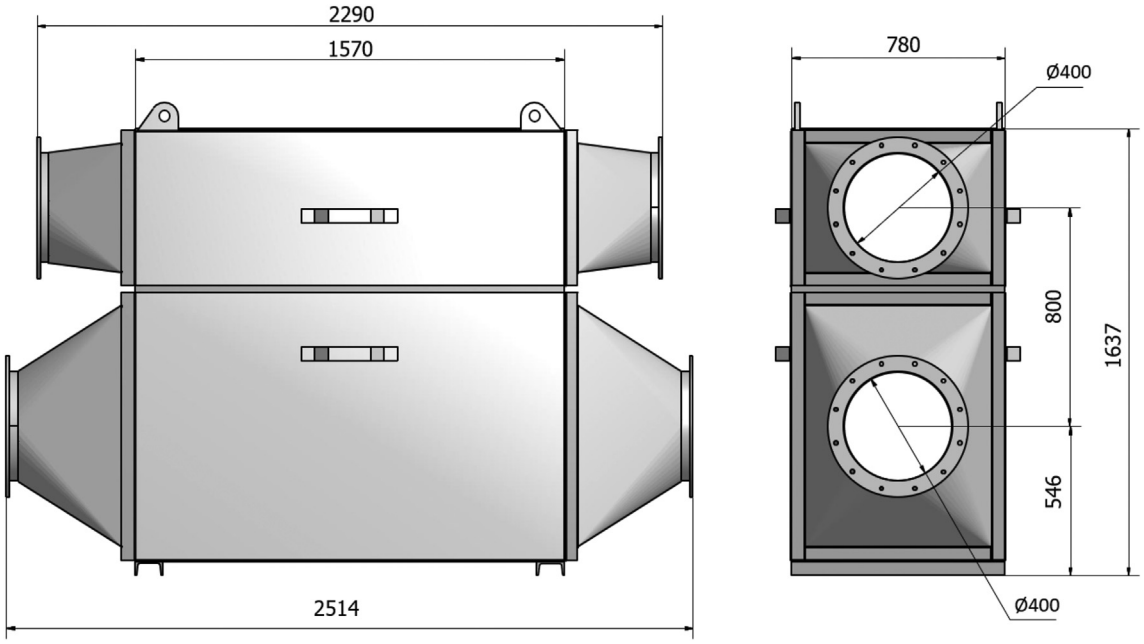

Fig. 8. Overall size HPHE.

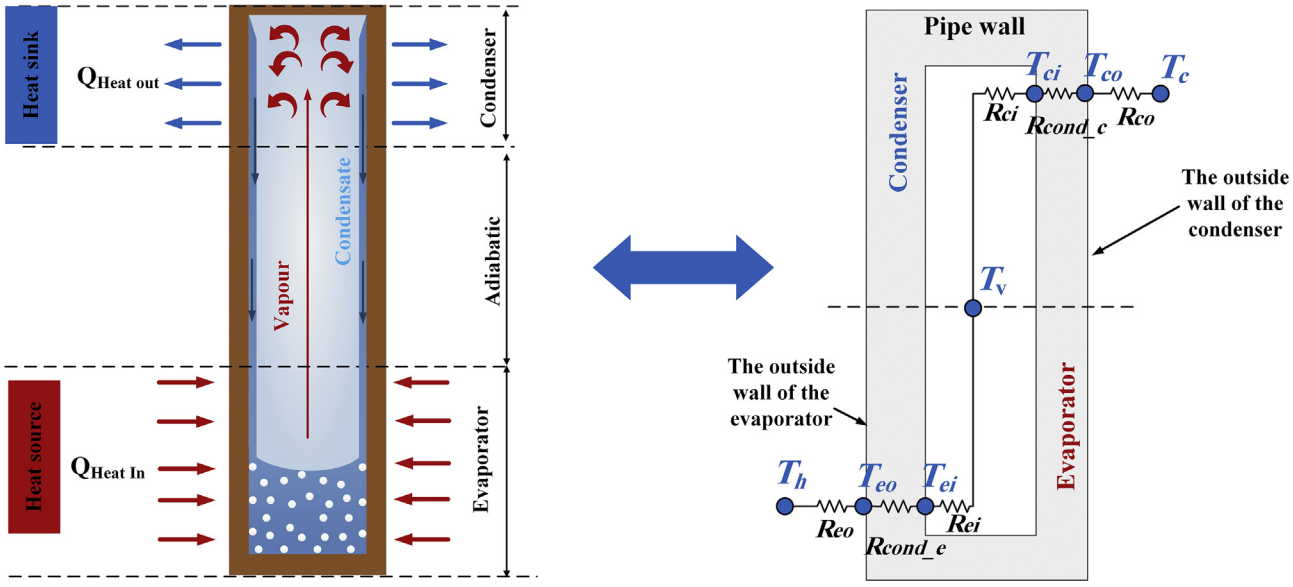

Fig. 9. Two-phase working cycle of a heat pipe and its corresponding thermal resistance model.

3.2. Theoretical modelling

The HPHE transfers the heat from the hot flue gas stream to the cold stream of air through the heat pipes. Each heat pipe transfers the heat separately, acting as an individual heat exchanger. The heat is transferred by forced convection from the hot flue gas to the outside of the heat pipe wall. Then it is transferred to the inside of the wall by conduction. The saturated liquid boils and the vapour flows up to the condenser due to a small pressure difference between the evaporator and the condenser. Then the saturated vapour condenses, releasing the heat to the inside of the condenser wall, and transferred to the outside of the wall by conduction. Finally, the heat is transferred from the outside of the condenser wall to the air by forced convection. The heat transfer process is analysed following the electrical analogy approach. In this approach, each thermal resistance is considered as an electrical resistance as illustrated in Fig. 9, and the main driving force is the temperature difference between the flue gas and the air stream.

The total thermal resistance of a single heat pipe, R_{hp}, can be obtained by Ref. [36]:

$$R_{hp} = R_{eo} + R_{cond\_e} + R_{ei} + R_{ci} + R_{cond\_c} + R_{co} \quad (1)$$

where R_{eo} and R_{co} are the forced convection heat transfer resistances at the evaporator and condenser, respectively. R_{cond_e} and R_{cond_c} correspond to the wall radial conduction at the evaporator and condenser, respectively. R_{ei} and R_{co} represent the boiling and condensation resistances of the heat pipe ($^{\circ}C \cdot W^{-1}$), respectively.

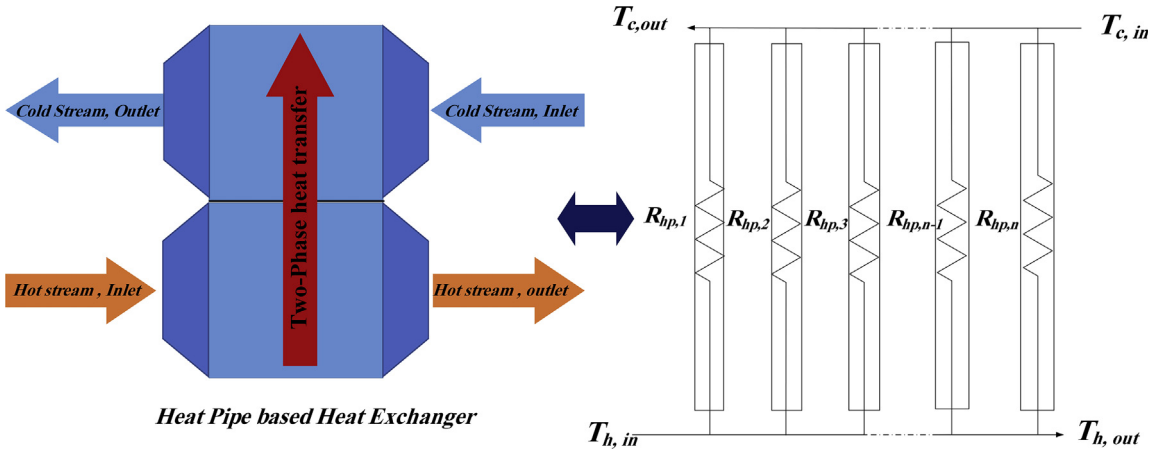

Fig. 10. Thermal electrical analogy of the heat pipe-based heat exchanger.

The boiling and condensation resistances are obtained from the relation between thermal resistance and heat transfer coefficient as follows:

$$R = \frac{1}{hA} \tag{2}$$

with R being the thermal resistance (°C. W^{-1}), h the heat transfer coefficient ($W.m^{-2}.°C^{-1}$), and A the heat transfer surface area (m^2).

The heat transfer coefficient for boiling was calculated from the correlation provided by *Rohsenow* [37] which is recommended for a wide range of applications [38]:

$$h_{boiling} = \mu_l.h_{fg}\left[\frac{g.(\rho_l-\rho_v)}{\sigma}\right]^{\frac{1}{2}}.\left[\frac{C_P}{\left(C_{sf}.h_{fg}.Pr_l^n\right)}\right]^3.(T_{ei}-T_v)^2 \tag{3}$$

where μ_l is the liquid dynamic viscosity (Pa.s), h_{fg} is the latent heat of vaporization ($J.kg^{-1}$), g is the gravitational acceleration ($m.s^{-2}$), ρ_l and ρ_v are the liquid and vapour densities ($kg.m^{-3}$), σ is the working fluid surface tension ($N.m^{-1}$), $Pr = \mu_l C_{P,l}/k_l$ is the liquid Prandtl number, C_P is the specific heat ($J.kg^{-1}.K^{-1}$), k_l is the thermal conductivity of the liquid ($W.m^{-1}.K^{-1}$),C_{sf} is a constant depending on the surface-fluid combination, and T_{ei} and T_v are the evaporator inner wall and the saturation temperature (°C), respectively.

The heat transfer coefficient for condensation is calculated using the *Nusselt* [39] correlation [40]:

$$h_{condensation} = 0.943\left[\frac{\rho_l(\rho_l-\rho_v)h_{fg}gk_l^3}{\mu_l L_c(T_{sat}-T_{ci})}\right]^{1/4} \tag{4}$$

where ρ_l and ρ_v are the liquid and vapour densities ($kg.m^{-3}$), h_{fg} is the latent heat of vaporization ($J.kg^{-1}$), g is the gravitational acceleration ($m.s^{-2}$), k_l is the thermal conductivity of the liquid ($W.m^{-1}.K^{-1}$), μ_l is the liquid dynamic viscosity (Pa.s), L_c is the condenser length (m), and T_{ci} is the temperature of the condenser wall (°C). The radial conduction resistances of the walls at the evaporator and condenser are given as follows:

$$R_{cond} = \ln(D_o/D_i)/(2\pi L_e k_e) \tag{5}$$

$$R_{c,cond} = \ln(D_o/D_i)/(2\pi L_c k_c) \tag{6}$$

D_o and D_i represent the external and internal diameters of the heat pipe (m), respectively. k_e and k_c are the wall thermal conductivity ($W.m^{-1}.K^{-1}$) at the evaporator and condenser, respectively, and L_e and L_c are the evaporator and condenser lengths, respectively (m).

The forced convection resistance at the evaporator $R_{e,out}$ and condenser $R_{c,out}$ can be expressed in terms of forced convection heat transfer coefficients and corresponding heat transfer area using Eq. (2). To determine the forced convection heat transfer coefficient of each pipe, the correlations by *Zukauskas* [41–43]can be used:

$$Nu = \frac{h_{F.convection}D_o}{k} = 0.192\left(\frac{\chi_t^*}{\chi_l^*}\right)^{0.2}\left(\frac{P_{fin}}{D_o}\right)^{0.18}\left(\frac{H_f}{D_o}\right)^{-0.14}Re^{0.65}Pr^{0.36}\left(\frac{Pr}{Pr_s}\right)^{0.25} \tag{7}$$

where Nu is the Nusselt number, $h_{F.convection}$ is the forced convection heat transfer coefficient ($W.m^{-2}.K^{-1}$),D_o is the external diameter of the heat pipe (m), k is the thermal conductivity of the fluid ($W.m^{-1}.K^{-1}$),χ_t^* is a ratio of transverse pitch to pipe diameter, χ_l^* is a ratio of longitudinal pitch to tube diameter, P_{fin} is the fin pitch, H_f is the fins height. Re is the Reynolds number, Pr and Pr_s are the Prandtl number of the flow and the Prandtl number at the surface temperature, respectively.

χ_t^* and χ_l^* are given by:

$$\chi_t^* = \frac{S_T}{D_o} \tag{8}$$

$$\chi_l^* = \frac{S_L}{D_o} \tag{9}$$

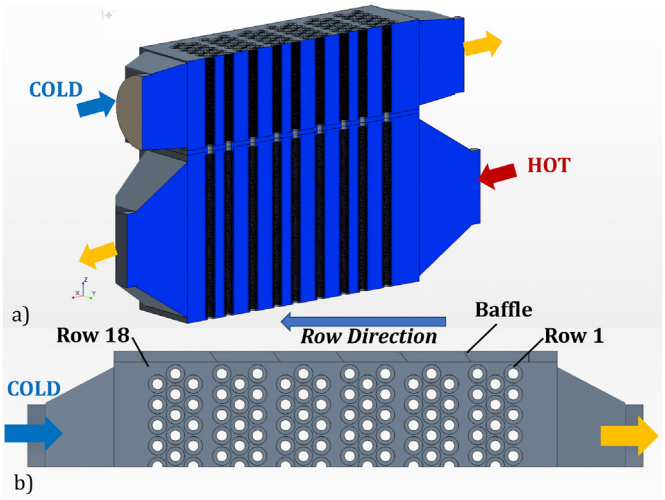

Fig. 11. (a) The geometry of the analysed convective HPHE, (b) condenser.

S_T and S_L are the transverse pitch and longitudinal pitch of the staggered heat exchanger (m).

The overall heat transfer area of the heat pipe for forced convection is calculated as follows:

$$A_{eo} = A_{eo,bare} + \eta_{eo} A_{eo,fins} \tag{10}$$

$$A_{co} = A_{co,bare} + \eta_{co} A_{co,fins} \tag{11}$$

where $A_{eo,bare}$ and $A_{co,bare}$ are the evaporator and condenser outer bare areas, respectively.$A_{eo,fins}$ and $A_{co,fins}$ are the fin surface areas and η_{eo} and η_{co} are the fin efficiencies at the evaporator and condenser, respectively.

The fin efficiency can be calculated from Ref. [44]:

$$\eta = \frac{\tanh\left(m_{fin}.Y_{fin}\right)}{m_{fin}.Y_{fin}} \tag{12}$$

where

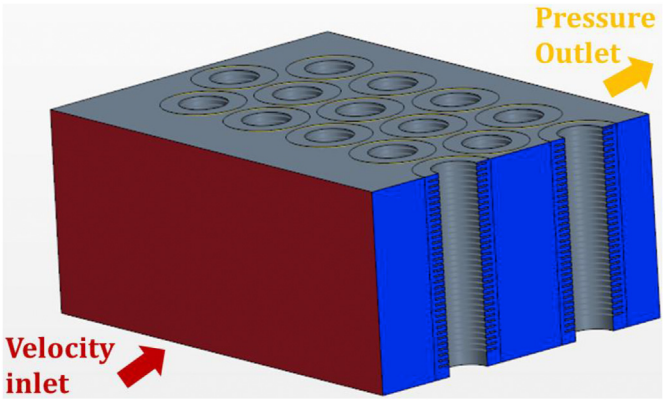

Fig. 13. Representative element considered for the mesh sensitivity analysis.

$$m_{fin} = \sqrt{\frac{2h_{F.convection}}{k_{fin}t_{fin}}} \tag{13}$$

$$Y_{fin} = \left(H_{fin} + \frac{t_{fin}}{2}\right)\left[1 + 0.35\ln\left(\frac{D_{fin}}{D_o}\right)\right] \tag{14}$$

with k_{fin} the thermal conductivity (W/m.K) of the fins and t_{fin} (m) the fin thickness.

As a result, the HPHE can be modelled based on the electrical analogy approach as presented in Fig. 10.

The heat recovery of the HPHE can be determined from the following equation [45]:

$$Q = \frac{\Delta T_{LM}}{R_{HPHE}} \tag{15}$$

where R_{HPHE} total is the overall thermal resistance of the HPHE. ΔT_{LM} is the logarithmic mean temperature of the inlet and outlet flue gas and air streams, which can be calculated for a counter flow heat exchanger from Ref. [46]:

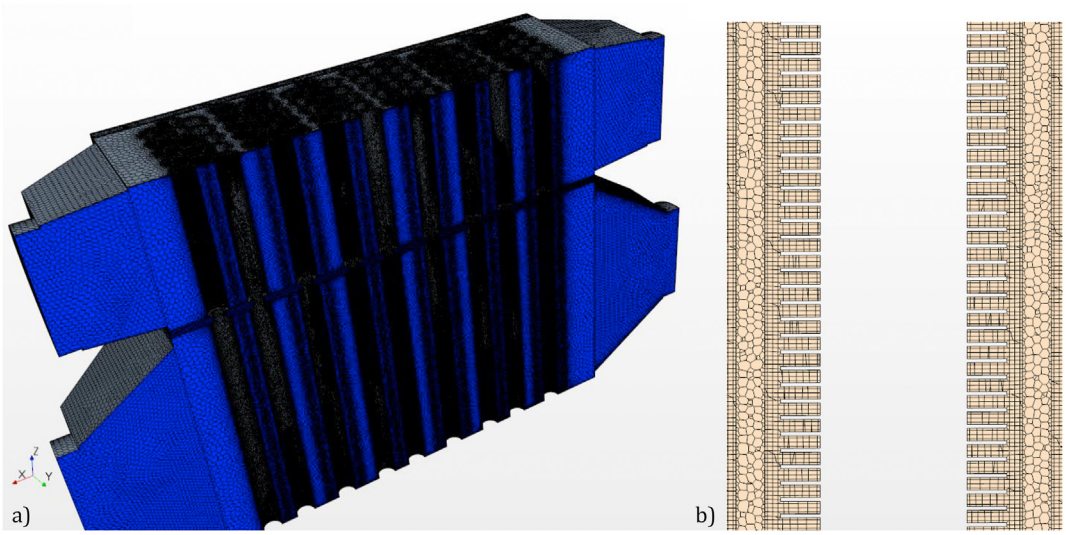

Fig. 12. (a) Computational domain of the convective heat exchanger (b) section of the mesh on a cut plane through the evaporator and a pipe of the first row.

Table 2
Pressure drop calculated with the four meshes considered.

Computational Grid#	Base Size/Minimum Size (mm)	N° of cells	Estimated N° of cells (Approx.)	Pressure Drop (Pa)
#01	28/2.8	1,118,565	50 million	78.0
#02	24/2.4	1,309,056	58 million	76.6
#03	20/2	1,557,485	70 million	75.6
#04	16/1.6	1,954,151	87 million	75.1

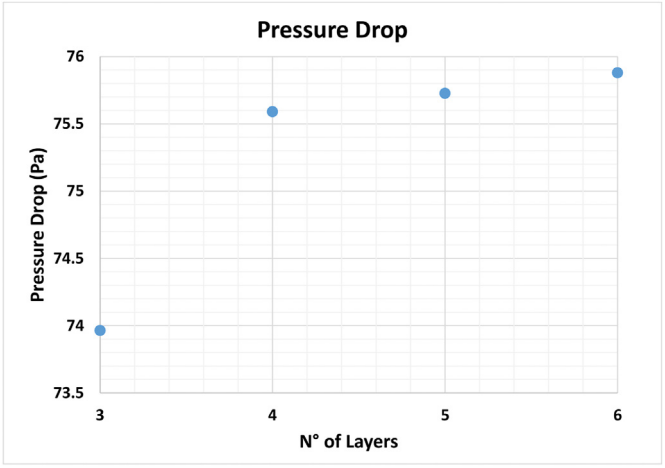

Fig. 14. Results of the mesh sensitivity analysis in terms of pressure drop for the considered computational fluid domain.

Table 3
Operating condition for the steady state analysis.

T_{in_hot} (°C)	FX_{in_hot} (kg.s^{-1})	T_{in_cold} (°C)	FX_{in_cold} (kg.s^{-1})
210.2	0.8061	33.1	0.3462

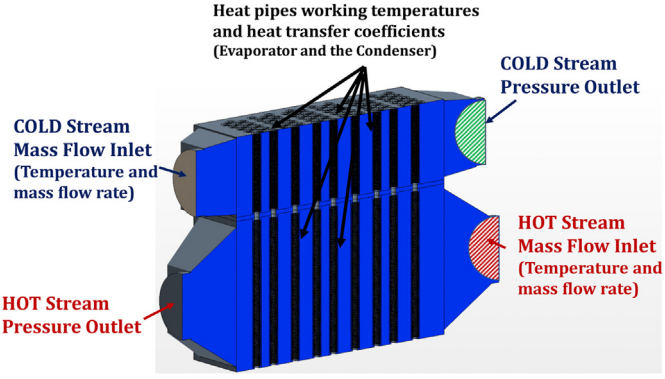

Fig. 15. Boundary conditions for the CFD simulation.

$$\Delta T_{LM} = \left(\frac{\left(T_{flue\ gas,in} - T_{air,out}\right) - \left(T_{flue\ gas,out} - T_{air,in}\right)}{\ln\left(\frac{T_{flue\ gas,in} - T_{air,out}}{T_{flue\ gas,out} - T_{air,in}}\right)} \right) \quad (16)$$

Eq.(*15*) can be written in a different form as follows:

$$Q = UA\Delta T_{LM} \quad (17)$$

where *UA* is the HPHE overall conductance (W/°C).

Based on the electrical analogy in Fig. 10, the total thermal resistance R_{HPHE} of the HPHE can be obtained from the following equation [47]:

$$\frac{1}{R_{HPHE}} = \frac{1}{R_{hp,1}} + \frac{1}{R_{hp,2}} + \ldots + \frac{1}{R_{hp,n-1}} + \frac{1}{R_{hp,n}} \quad (18)$$

where R is the thermal resistance (°C/W), the subscripts *hp* refers to heat pipe, and n is the number of heat pipes in the heat exchanger. Assuming that the resistance is equal for all the heat pipes, the total thermal resistance R_{HPHE} of the heat pipe heat exchanger can be expressed as:

$$R_{HPHE} = \frac{R_{hp}}{n_{total}} \quad (19)$$

with R_{hp} the average resistance of a heat pipe (°C/W), and n the number of heat pipes in the heat exchanger.

The heat transfer rate can be calculated from:

$$Q = \dot{m}_{air} C_{P,air} \left(T_{air,in} - T_{air,out}\right) \quad (20)$$

The effectiveness of a heat exchanger is the ratio of the actual heat transfer rate to the maximum theoretically possible heat transfer rate.

The effectiveness (ε) of the HPHE is given by the following expression [48]:

$$\varepsilon_{HPHE} = \frac{Q_{air}}{Q_{max}} \quad (21)$$

Q_{air} is the actual heat transfer rate recovered (W), and Q_{max} is the maximum possible heat transfer rate (W). The maximum heat transfer rate achievable by a heat exchanger depends on the inlet

Table 4
Operating parameters (temperatures and heat transfer coefficient) of the heat pipes in the evaporator (boiling) and condenser (condensation).

Row Number	Working Temperature (°C)	Heat Transfer Coefficient (**W**.**m**$^{-2}$.**K**$^{-1}$)	
		Evaporator	Condenser
1	201.33	1675.49	9183.76
2	198.97	1738.03	9107.65
3	196.40	1797.51	9012.32
4	193.62	1856.17	8917.22
5	190.59	1913.54	8822.12
6	187.29	1969.16	8726.66
7	183.72	2022.64	8629.76
8	179.84	2073.06	8532.51
9	175.63	2119.98	8434.22
10	171.06	2162.60	8334.10
11	166.11	2200.05	8231.48
12	160.75	2231.35	8126.46
13	154.95	2255.63	8016.78
14	148.69	2271.51	7902.07
15	141.92	2277.85	7781.61
16	134.62	2273.21	7653.53
17	126.76	2255.93	7516.68
18	118.32	2224.41	7369.06

temperatures of both fluids and of the minimum heat capacity rate of the fluids as follows:

$$Q_{max} = C_{min}\left(T_{flue\ gas,in} - T_{air,in}\right) \quad (22)$$

In this expression, C_{min} is the minimum heat capacity rate ($W \cdot K^{-1}$), and $T_{flue\ gas,\ in}$ and $T_{air,in}$ are the inlet temperatures of the flue gas and air streams, respectively. Eq. (22) stipulates that the maximum heat transfer achievable is the case where the fluid with minimum heat capacity reaches the temperature of the other fluid. Indeed, the heat capacity rate indicates the capacity of a fluid to increase its temperature for a given heat transfer rate. In this study, the fluid with minimum heat capacity rate was the air. Thus, the minimum capacity rate C_{min} can be written as:

$$C_{min} = \dot{m}_{air} C_{P,air} \quad (23)$$

where $\dot{m}_{air}$ is the air mass flow rate ($kg.s^{-1}$), and $C_{P,air}$ is the specific heat of air ($J.kg^{-1}.K^{-1}$).

3.3. CFD analysis

The numerical modelling of the heat pipe heat exchanger is carried out by means of the computational fluid dynamics code StarCCM+ 13.06.012 licensed by Siemens. Fig. 11 displays the real geometry of the analysed heat pipe heat exchanger that includes the following components: the evaporator, the separation plate, the condenser, the inlet and outlet ducts and the heat pipes. The investigated system includes 18 rows of heat pipes with 9 pipes per row; in order to increase the heat exchange area, the pipes incorporate fins that are included in the calculation. The geometry includes baffles in correspondence with each group of heat pipes in order to direct the fluid across the heat pipes. Fig. 11 (b) displays the baffles for the condenser; in the evaporator the deflectors are placed on the reverse side. The computational domain highlighted in Fig. 11 takes advantages of a plane of symmetry present in the flow; for this reason, half geometry is used in the analysis due to the symmetry with respect to the longitudinal section.

Particular care is devoted to the mesh construction and the heat transfer modelling between the pipes and the air flows in the primary and secondary streams. For the air, an ideal gas approach is used for the simulation and the energy balance equation is solved for the enthalpy. Turbulence is accounted for in the simulation by means of the two-equation k-omega approach [49]. Fig. 12 displays the computational grid adopted for the simulation. The grids of the evaporator and the condenser, shown in Fig. 12 (a), are constructed using a polyhedral mesh. The average size of the mesh is 20 mm with proper refinement, i.e. 2 mm, in the regions where the fluid flows across the pipes. The computational domain of the heat pipe fins is discretized using a Thin Mesher with an average base size of 20 mm and a minimum size of 2 mm on the fin surfaces orthogonal to the fins' thickness: as it can be seen from Fig. 12 (b), 4 layers have been generated in the volume distribution, i.e. direction of the fin thickness. The grid of the separation plate is constructed using a polygonal mesh with a base size of 4 mm and 8 layers in the volume distribution, while the inlet and outlet ducts are obtained with a polygonal mesh, i.e. 20 mm base size. The total number of cells of the entire domain of the convective heat exchanger is 66,829,162 (see Table 1).

Different grid sizes have been tested and a mesh sensitivity analysis was conducted for an elementary element which is representative of the entire geometry; this element, depicted in Fig. 13, accounts for a section of 15 pipes and its volume is equal to a forty-fifth of the entire geometry. In this case, the air flow enters with a velocity imposed equal to 5 m s^{-1}. Table 2 shows the four different meshes analysed with an average grid spanning from 28 to 16 mm for the evaporator and condenser regions. The estimation of the number of cells of the entire calculation domain results in 50, 58, 70 and 85 million cells. The results in terms of pressure drop across the representative element investigated are reported in the same table. The error introduced by the coarse mesh is approximately 3.4% with the respect to the finest grid, while the error between the grid#3 and grid#4 is approximately the 0.6%. Thus, the computational grid#3 can be considered adequate for the simulation of the case tested.

The influence on the accuracy of the results of the variation in the fin's number of layers in the volume distribution is investigated for the computational grid#3. The four computational grids investigated are characterized by 3, 4, 5 and 6 layers in the pace between two fins of the same heat pipe. Fig. 14 displays the dependency of the results on the number of layers in terms of pressure drop. No remarkable differences are calculated in terms of pressure drop for the grid with 4, 5 and 6 layers, i.e. less than 0.4% between the configurations with 4 and 6 layers. The mesh selected in the simulation, i.e. 4 layers, results to be the best trade-off between the results' accuracy and computational effort.

Boundary conditions.

The performance of the convective heat exchanger is determined under the reference working condition and assuming steady state operation. Table 3 lists the design parameters of the heat exchanger. In this case, the temperature of the gas at the inlet of the evaporator is 210 °C while the inlet temperature of the condenser is 33 °C.

The data reported in Table 3 are used as input values for the mass flow rate boundaries of the CFD simulation, as displayed in Fig. 15.

The effect of the boiling and condensation heat transfer that takes place inside the heat pipes is also included in the analysis using the convection boundary condition available in StarCCM+, which calculates the thermal exchange from the environment, i.e. ambient inside the heat pipes, to the external side of a boundary, i.e. fluid domain of the evaporator and the condenser (see Fig. 15). The "convection boundary condition feature" requires specifying the temperature and the heat transfer coefficient ($W/m^2.K$) for the environment that is, in this simulation, the ambient inside of the heat pipes. Therefore, the temperature to be set is the working temperature of the heat pipes and it can be considered the same for the heat pipe boundaries of the evaporator and condenser, since it is assumed that the working cycle of the heat pipes is at steady state; the heat transfer coefficient set in the software is different for the boundaries of the evaporator and the condenser because it accounts for the contribution of the evaporation and the condensation inside the heat pipes. Due to the fact that the heat pipe walls are not considered in the simulated geometry, the heat transfer coefficients set in the software accounts for the contribution of the conduction in the walls, according to the following equations:

Equation for the heat pipe wall boundaries in the evaporator:

$$K_e = \frac{1}{A_{1e} + \eta A_{2e}} \times \frac{1}{\frac{1}{h_{ei}A_{ei}} + \frac{\ln\left(D_o/D_i\right)}{2\pi L_e k}} \quad (24)$$

Equation for the heat pipe wall boundaries in the condenser:

$$K_c = \frac{1}{A_{1c} + \eta A_{2c}} \times \frac{1}{\frac{1}{h_{ci}A_{ci}} + \frac{\ln\left(D_o/D_i\right)}{2\pi L_c k}} \quad (25)$$

where K_e is the equivalent heat transfer coefficient for the

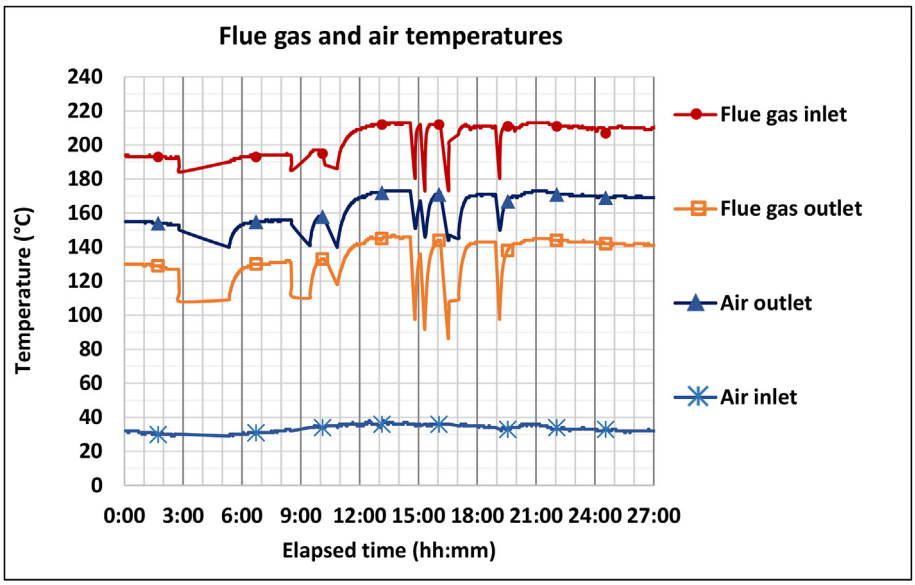

Fig. 16. Heat pipe heat exchanger temperatures during 27 working hours.

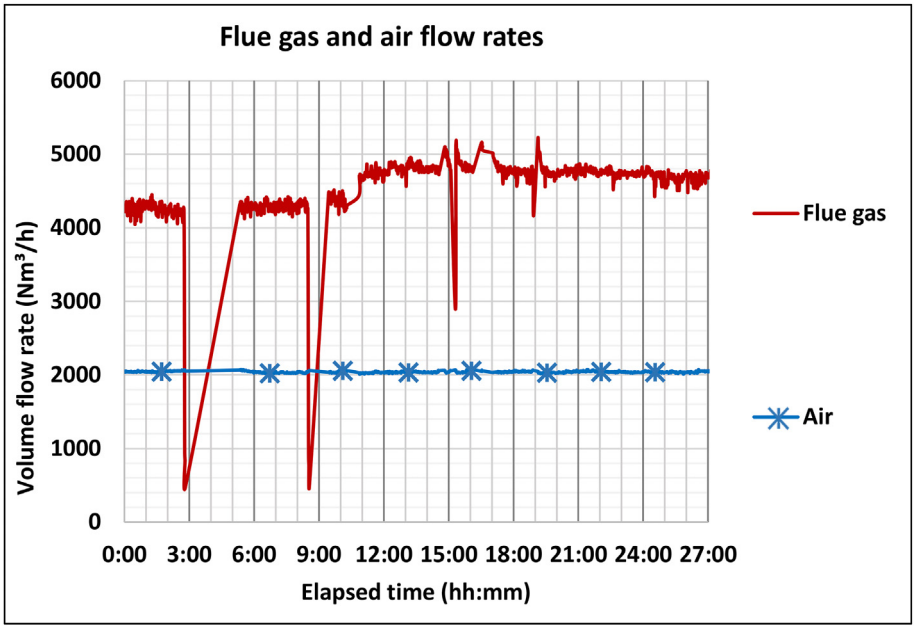

Fig. 17. Flue gas and air flow rate measurements.

evaporator wall boundary. FX is the heat transfer coefficient for boiling phenomenon $(W.m^{-2}.K^{-1})$. K_c is the equivalent heat transfer coefficient accounting for the condenser wall boundary. FX is the heat transfer coefficient for condensation FX, A_{ei} and A_{ci} are the internal areas of the heat pipes in the evaporator and in the condenser, FX is the thermal conductivity of the walls $\left[\frac{W}{m*K}\right]$, A_{1e} and A_{1c} are the bare areas for the heat pipes respectively in the evaporator and in the condenser (m2), A_{2e} and A_{2c} are the fin areas for the heat pipes respectively in the evaporator and in the condenser section (m^2). η is the fin efficiency.

Table 4 summarizes the values calculated and used in the simulation for the heat transfer coefficients and the saturation temperatures for each row of the heat pipes, both in the evaporator and in the condenser. The heat transfer coefficients reported in the Table account for the contribution of conduction in the heat pipe walls and the boiling and condensation phenomena, respectively, in the evaporator and in the condenser.

Furthermore, the thermal exchange with the external ambient is also addressed in the simulation in order to simulate the convective heat exchange between the external walls of the HPHE and the external ambient. The temperature of the ambient is set at 25 °C.

3.4. HPHE return on investment (ROI)

The HPHE was evaluated financially using the return on investment metric (*ROI*). *ROI* can be calculated from the following formula [18]:

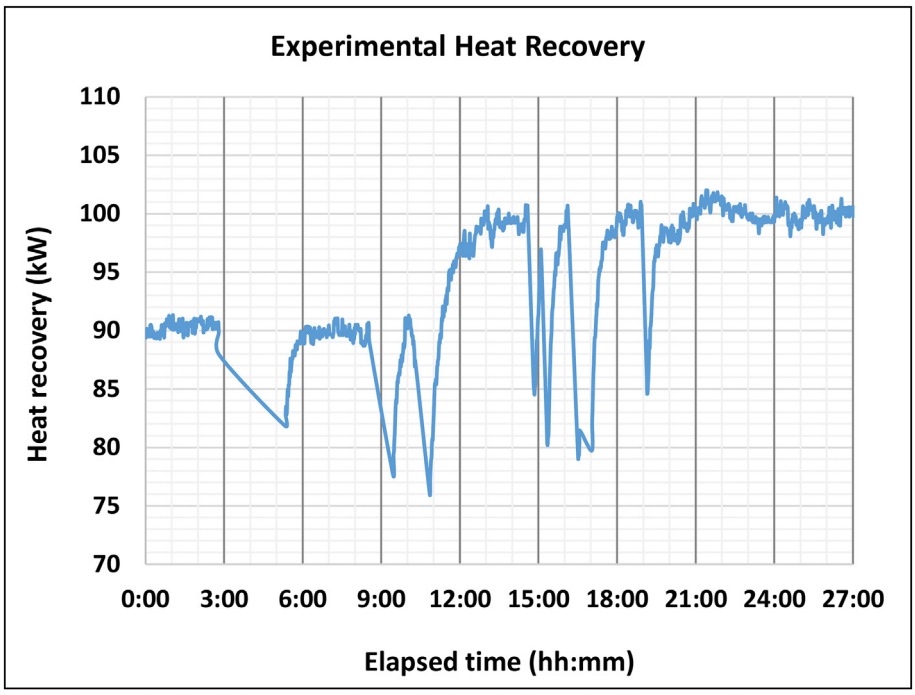

Fig. 18. Experimental heat recovery during 27 working hours test.

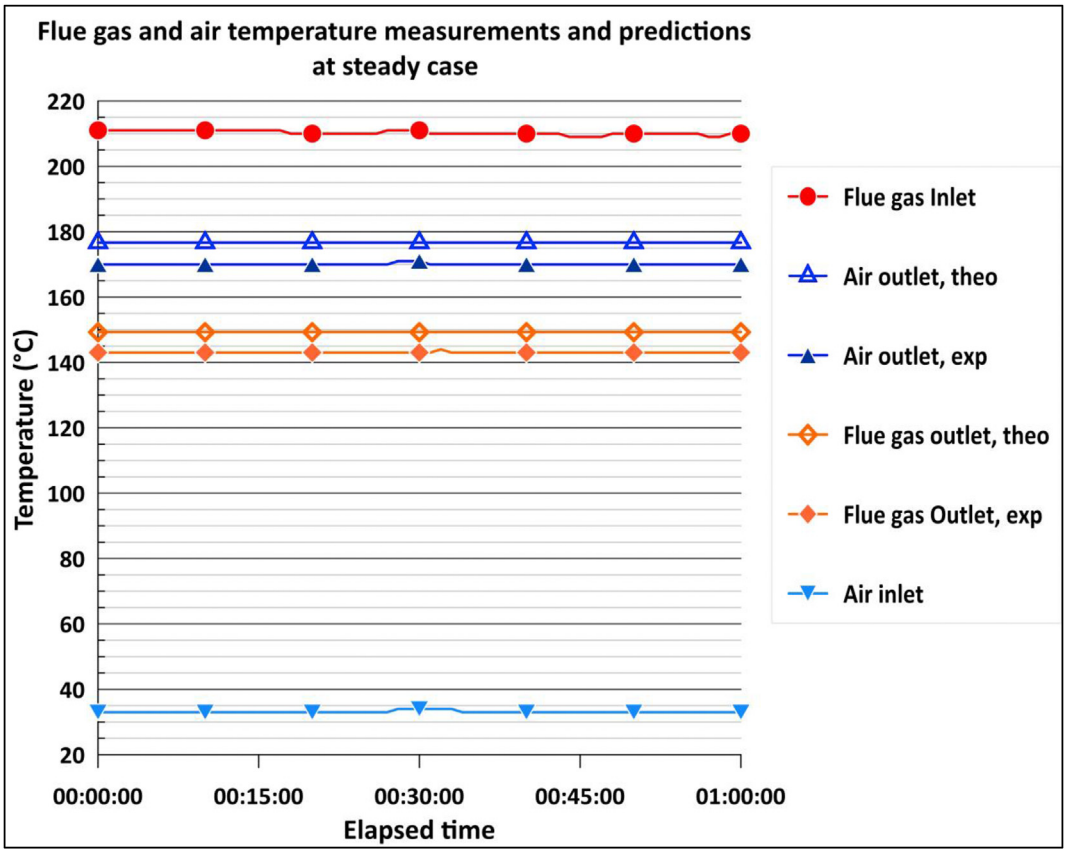

Fig. 19. Flue gas and air temperature at steady state.

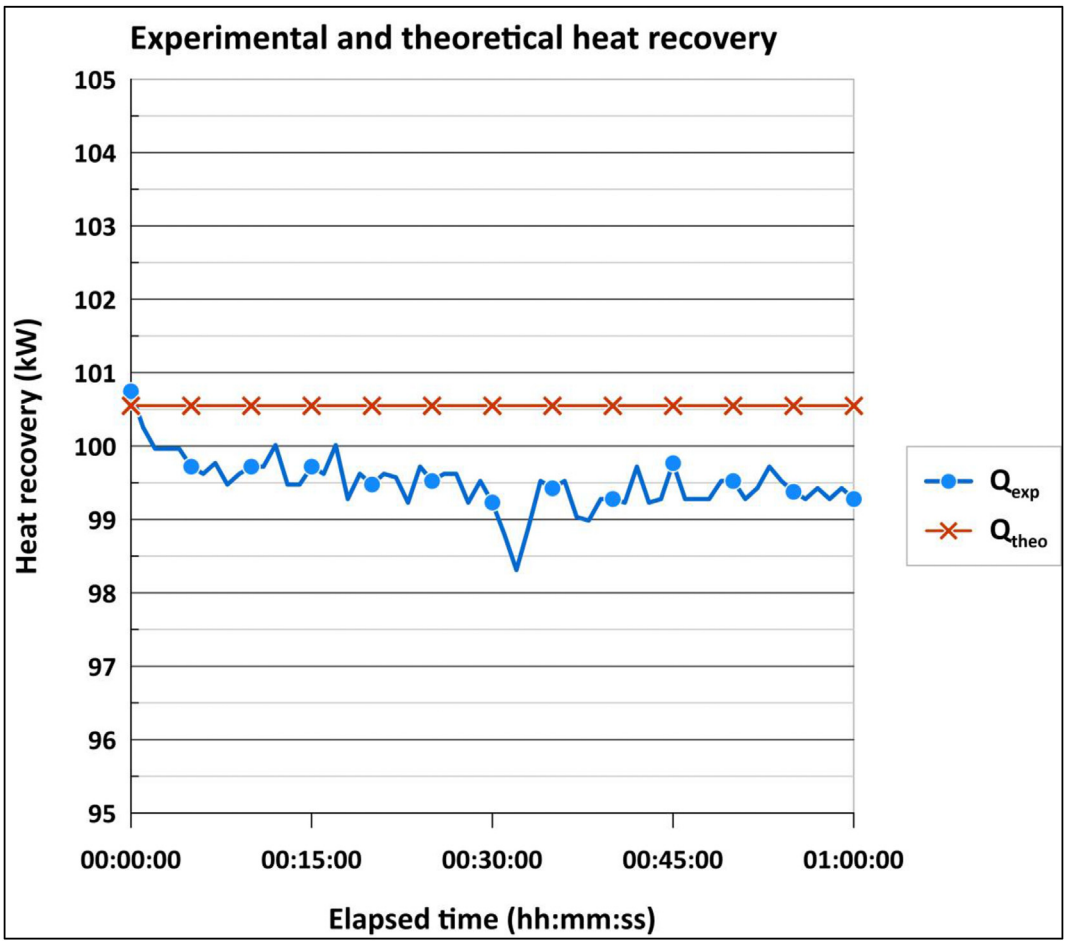

Fig. 20. Experimental and theoretical heat recovery during steady state conditions.

$$ROI = \frac{Net\ Profit}{Cost\ of\ Investment} \times 100 \quad (26)$$

Another financial figure to evaluate the investment is the payback period which is presented as follows:

$$Payback\ period = \frac{Cumulative\ Cash\ Flow}{Annual\ Net\ Benefit} \times 12\ (months) \quad (27)$$

The net profit is normally calculated per annum; hence *ROI* measures the percentage of gain per annum as well.

The cost of investment is the sum of the HPHE capital cost and installation cost. The net profit is obtained from the equivalent cost of heat recovered as a fuel cost and savings in the reduction of CO_2 trade price.

$$E_{HPHE} = \dot{Q}_{HPHE} \times R_{time,\ HPHE} \quad (28)$$

The additional energy saving due to utilising the HPHE as an alternative heat source instead of using a burner is calculated as follows:

$$E_{extra} = (1 - \eta_{burner})\dot{Q}_{HPHE} \times R_{time,\ HPHE} \quad (29)$$

The efficiency of the burner varies between 0.85 and 0.99 depending on its design, $R_{time,\ HPHE}$ is the working hours of the HPHE per year.

Reduction in natural gas saving per year can be calculated from:

$$Cst_{CO_2,reduction} = m_{CO_2} \times cst_{CO_2,trade\ price} \quad (30)$$

$cst_{CO_2,trade\ price}$ is the trade price of CO_2 emission per kg, and m_{CO_2} is the mass of CO_2 saved per year due to utilising the HPHE.

The net profit can be calculated from:

$$Net\ profit = (E_{HPHE} + E_{extra}) \times Cst_{NG} + Cst_{CO_2,reduction} - Cst_{O\&M} \quad (31)$$

Cst_{NG} is the cost of natural gas per kWh, and $Cst_{O\&M}$ is the cost of maintenance due to operating the HPHE, which is minimal, such as replacing consumables, as the HPHE does not require any specific maintenance.

4. Results and discussion

4.1. Experimental results

The data were collected for a prolonged time, over 27 h. The inlet and outlet temperatures of the flue gas and the air stream measurements are presented in Fig. 16. Flue gas and air stream flow rates are presented in Fig. 17. The kiln experienced some variation in the operating mode during the test, which can be seen as a small temperature drop in the flue gas inlet in Fig. 16, and a sudden drop in the flue gas flow rate from 4300 $Nm^3.h^{-1}$ to 400 $Nm^3.h^{-1}$, as shown in Fig. 17. However, the fans were still functioning to provide air to the dryers located after the condenser section with a volume

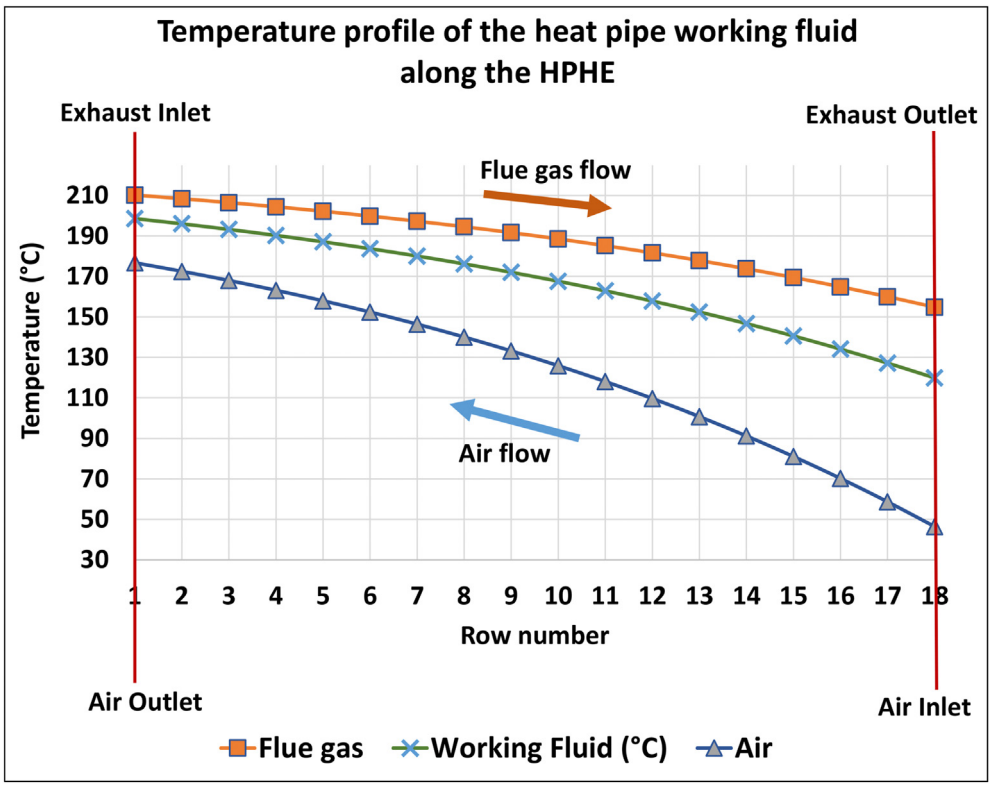

Fig. 21. Row by row thermal performance predictions of the HPHE.

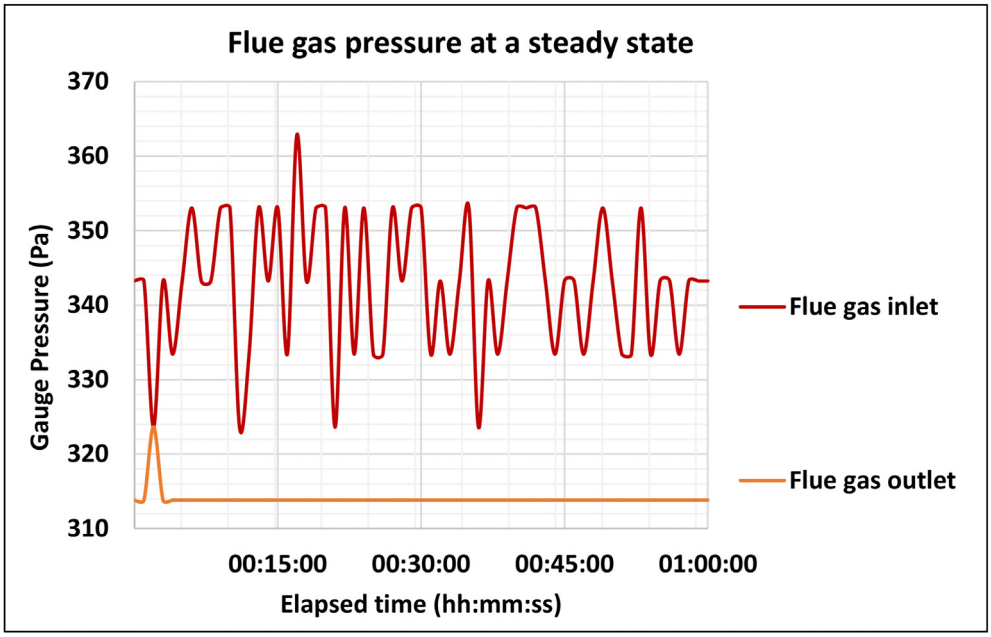

Fig. 22. Flue gas pressure measurements.

flow rate of 2000 $Nm^3.h^{-1}$. As a result, the flue gas and air outlet temperatures also decreased. It can be observed that the HPHE had a quick response time as the flue gas outlet temperature dropped instantly with the drop of the flue gas flow rate. However, the air outlet temperature declined linearly, showing a thermal lag as the flue gas flow rate rose again, due to the thermal diffusivity of the heat pipes.

The flue gas inlet temperature varied between 180 °C and 210 °C, while the flue gas outlet temperature varied between 110 °C and 145 °C. The air inlet temperature was around 30 °C during the tests, while the air outlet temperature varied between 140 °C and 170 °C. It can be noticed that the air outlet temperature was higher than the flue gas outlet temperature due to the counter-current design of the HPHE, and since the air flow rate was two times

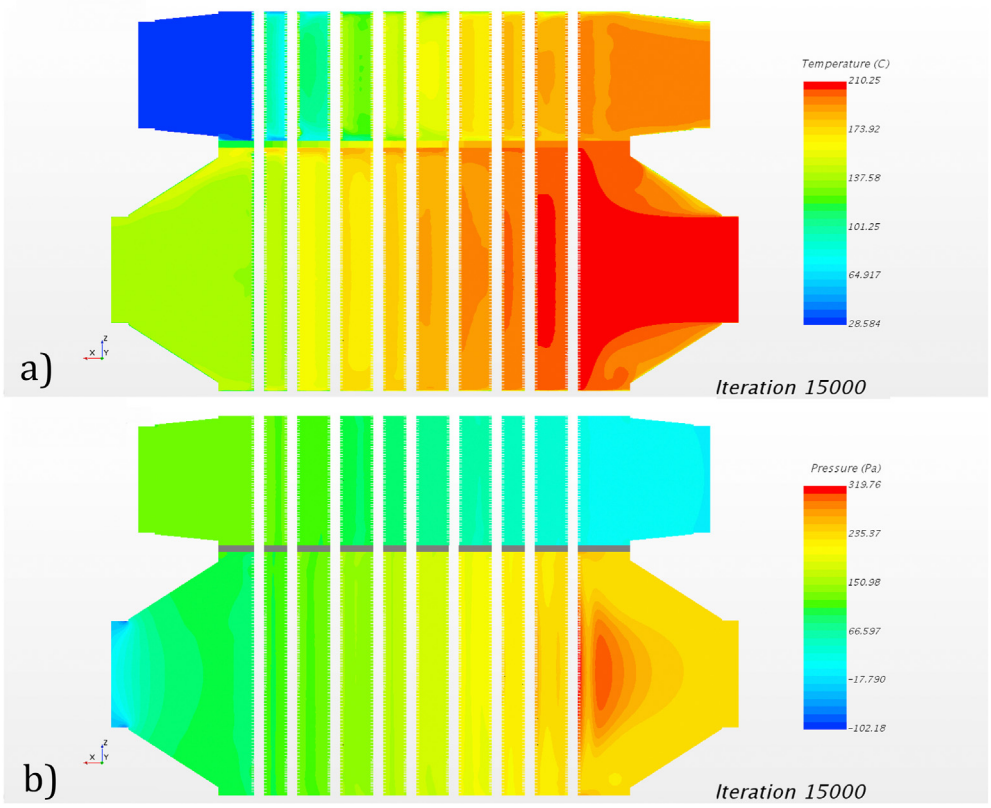

Fig. 23. (a) Temperature distribution and (b) pressure distribution on the plane of symmetry of the evaporator and the condenser.

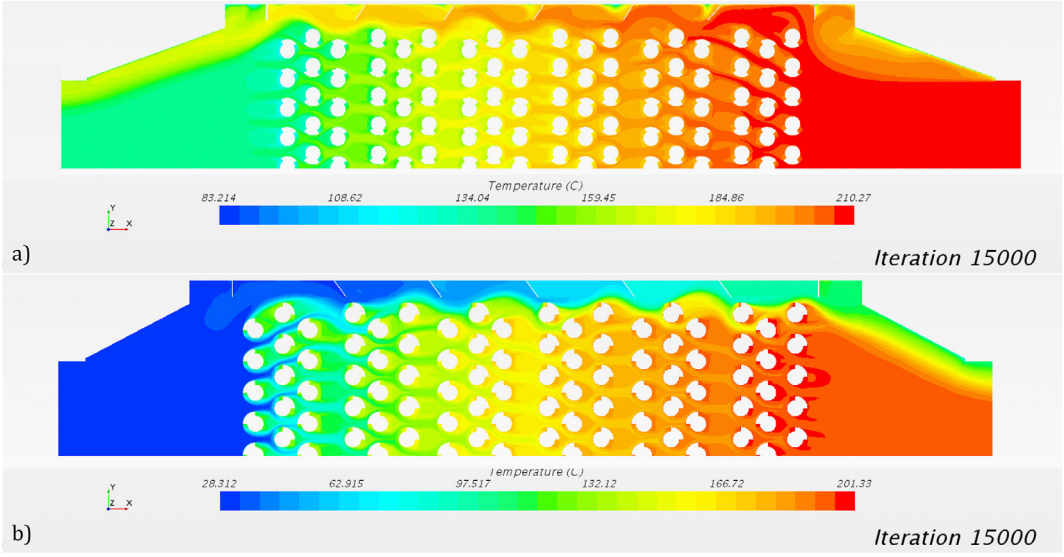

Fig. 24. Temperature distribution (a) on a section through the evaporator and (b) on a section through the condenser.

less than the flue gas flow rate.

A similar trend can be seen in Fig. 18, which represents the heat recovered by the system over the test period. The heat recovery varied between 76 kW and 103 kW depending on the kiln operating conditions. It can be seen that the maximum heat recovery was obtained when the system was at steady state.

4.2. Theoretical modelling results

The theoretical results were compared with the experimental data at steady state conditions for a duration of 1 h. The experimental values of the inlet temperatures and flow rates of the flue gas and the air were input into the theoretical model, to predict the thermal performance of the HPHE. The HPHE model predictions of the outlet temperatures of the flue gas and air are compared with

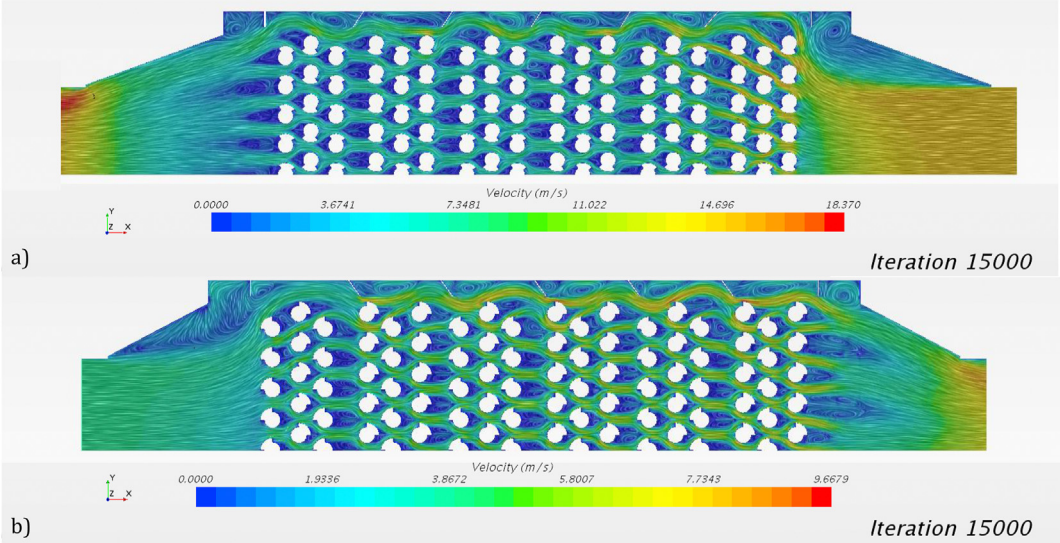

Fig. 25. Velocity distribution (a) on a section through the evaporator and (b) on a section through the condenser.

the measurements in Fig. 19. The flue gas outlet temperature was 143 °C while the model predicted a temperature of 149.3 °C. The air outlet temperature was 170 °C, while the model predicted the temperature to be 176.7 °C.

The experimental and theoretical heat recovery during steady state conditions of flow rate and inlet temperatures are presented in Fig. 20. The experimental heat recovery was around an average value of 99.5 kW ± 0.5 kW, while the theoretical heat recovery was 100.5 kW based on the inlet measurements.

The temperature changes of the HPHE flue gas and air streams along the HPHE are presented in Fig. 21. The temperature changes were calculated using the theoretical model, allowing for thermo-physical properties changes after each row. The temperature difference between flue gas and air was decreasing in the direction of air flow, and it shows that the air temperature rose to get close to the flue gas temperature at the air outlet. The effectiveness of the HPHE, ϵ, was 81% and the *UA* value of the HPHE was 1512 W °C^{-1}. The heat pipe working temperature was closer to the flue gas temperature than to the air temperature, depending on the heat pipe and HPHE geometry and the heat transfer coefficient at each stream. It can be also observed that the heat pipe working temperature was changing with each row in a similar trend to that of the flue gas temperature. The working fluid pressure inside the heat pipes varied between 2 and 15 bar depending on the working temperature of the heat pipes as plotted in Fig. 21.

The flue gas pressure measurements at the inlet and outlet of the HPHE during the thermal steady state are plotted in Fig. 22. The flue gas inlet pressure was fluctuating between 322 Pa gauge pressure and 363 Pa gauge pressure. The flue gas pressure after the HPHE was 314 Pa (gauge pressure). The fluctuation in the pressure measurements could be caused by flow turbulence in the region between the fan and the HPHE where the pressure sensor was placed. The pressure drop due to the hydraulic resistance of the HPHE was measured to be 40 Pa.

4.3. CFD results

Temperatures, pressures and the velocity field obtained by the CFD study of the evaporator and the condenser are reported and the recovered heat is determined. Fig. 23 shows the results in terms of temperature distribution, Fig. 23(a), and pressure distribution, Fig. 23(b), on the plane of symmetry after 15,000 steps. As expected, it can be noticed that in the evaporator the temperature decreases from the initial value of 210 °C to approximately 145 °C, when the fluid flows across the heat pipes; in the condenser, the outlet temperature is approximately 180 °C. Similarly, the maximum pressure can be registered at the inlet both in the evaporator and in the condenser; the heat pipes and the baffles represent the main contribution for the pressure loss in both streams.

Fig. 24 and Fig. 25 show the results in terms of temperature and velocity distribution for the simulated operating condition. The temperature and the velocity are displayed on two sections through the central part of the evaporator and the condenser. Analysing the temperature results in Fig. 24, cold spots in the evaporator and hot spots in the condenser can be observed in the proximity of the heat pipes; in these regions the fluid temperature reaches the working temperature of the heat pipes. It can be seen that the fluid is well distributed in the section of the evaporator in Fig. 25 (a), and in the condenser in Fig. 25 (b). A significant volume of air can be identified in both planes in the area between the last heat pipes in the rows and the heat pipe inspection doors. The portion of uncooled flue gas can be also identified in Fig. 24 (a), while at the condenser section, the air close to the wall is not heated up, as shown Fig. 24 (b). The average temperature at the outlets of the evaporator and the condenser are shown in Fig. 26 (a): the temperature at the evaporator outlet is 147 °C while the temperature at the condenser outlet is 178 °C. The thermal power transferred in the evaporator is 51,360 W while the thermal power recovered in the condenser is 50,678 W, see Fig. 26 (b); since in the simulation it has been considered half of the real geometry, the numerical results of the thermal power are twice these values.

4.4. Return on investment results

The installed system acted as a baseline HPHE model highlighting the potential for a HPHE system within the ceramic industry. The system as a whole defines the potential of replicability of the technology to have a payback period of less than 3 years. Fig. 27 highlights the payback period of 15 months with the currently installed HPHE unit. The breakdown of the initial investment, power recovered, and operational time is defined in

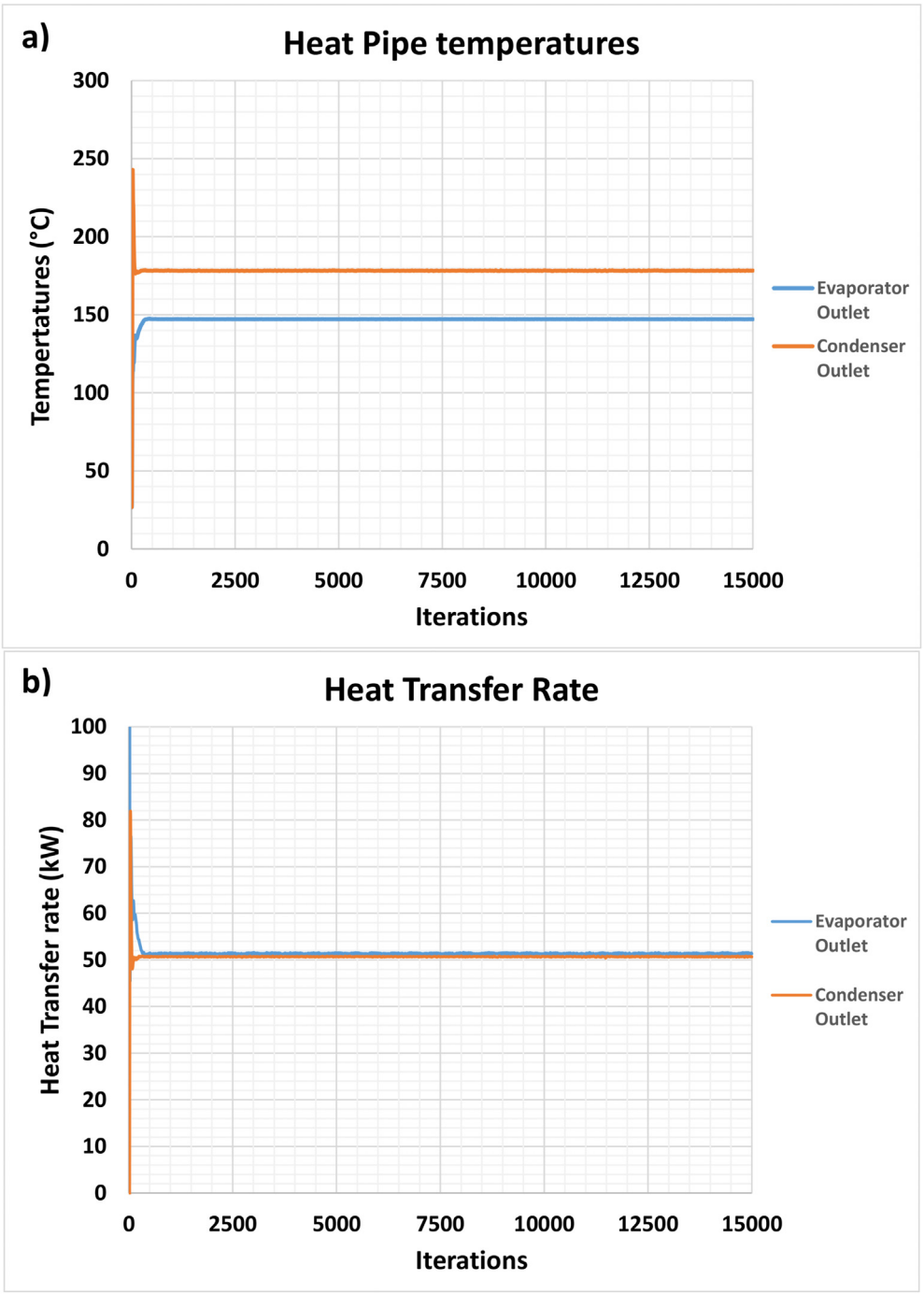

Fig. 26. (a) Temperature time histories of the evaporator outlet and the condenser outlet and (b) Thermal power time histories recovered by the evaporator and the condenser.

Table 5. It can be noted that due to the nature of the test set up, the installation cost has been omitted.

The large-scale development and production of the Heat Pipe Heat Exchanger on a commercial level significantly reduces the unit cost due to the optimization of design and manufacturing techniques for mass production. The following section will calculate the *ROI* on the basis of a fully disseminated unit suitable for mass implementation within the ceramic industry. Fig. 28 reflects the *ROI* of the optimised unit, with an *ROI* of 16 months. The slight increase in *ROI* compared to the currently installed system reflects the addition of the installation cost. A breakdown of the initial investment, power recovered and running time is given in Table 6.

4.5. Discussion

The HPHE exhibited a fast response to changes in the inlet temperature and flow rate of the flue gas stream. The theoretical results were in excellent agreement with the experimental results with less than 10% error. The variance between the outlet temperature measurements and the theoretical predictions was less than 7 °C which depends on both the error of the heat recovery prediction and the heat capacity rate of the fluid. The accuracy of

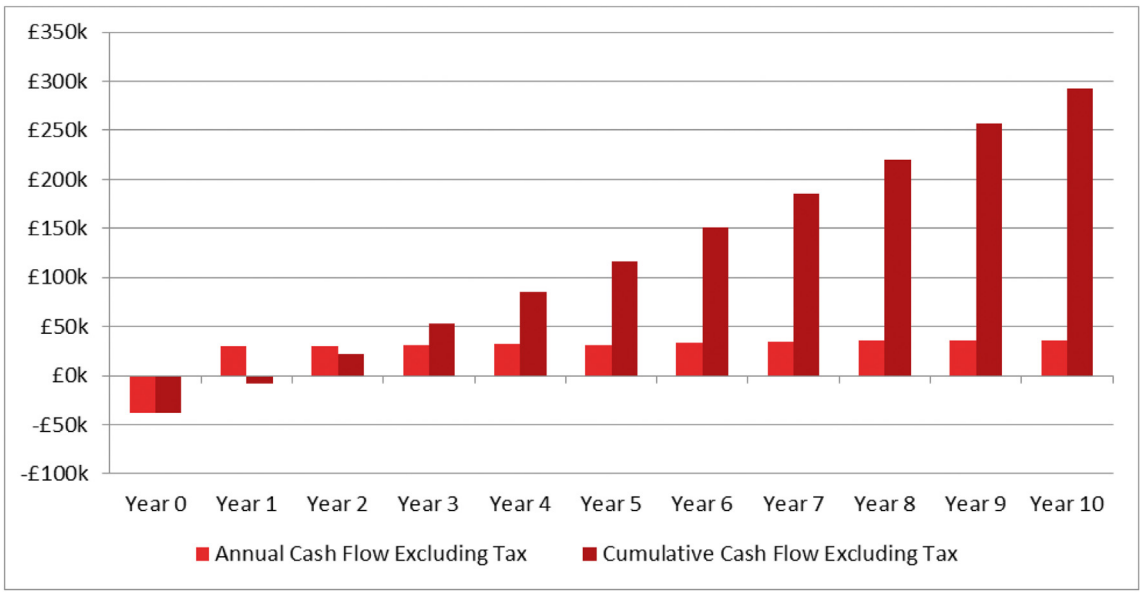

Fig. 27. Cash flow of installed unit.

Table 5
Investment evaluation.

Installation Main Data		
Total Investment	£	38,000
Power Recovered & Used	kW	100
Additional Power Savings	kW	15
Working Hours per Year	h	8760
Investment Evaluation		
Simple Payback Period		15 Months

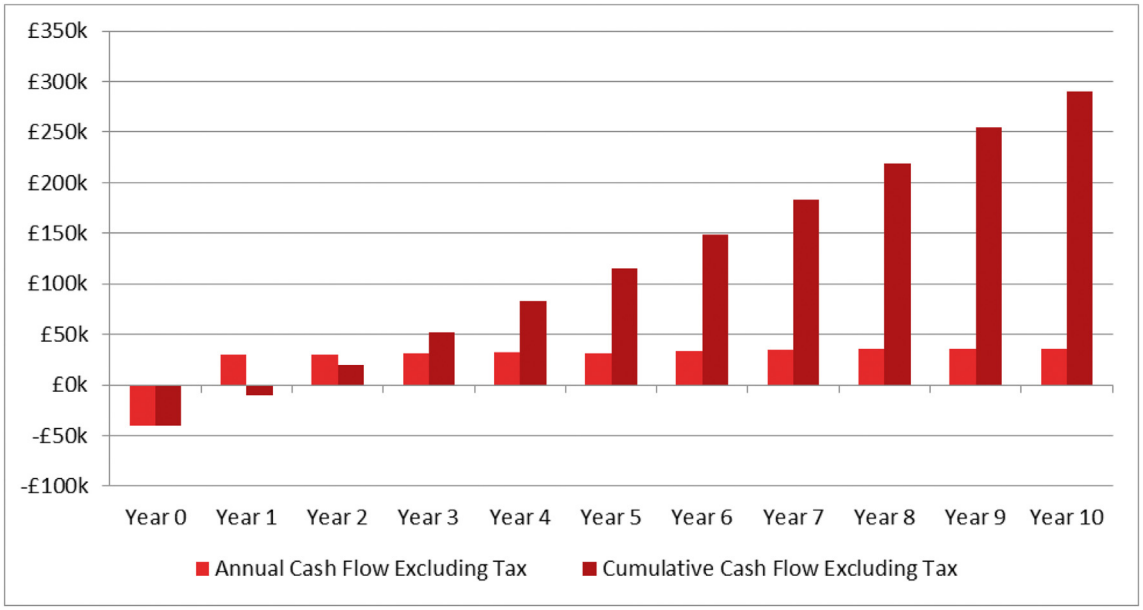

Fig. 28. Cash flow of optimised unit.

the model depends on the correlations used to calculate the thermal resistances and approximations made in order to program the model.

The detailed calculation of the flow field in the heat pipe heat exchanger gives an opportunity to calculate accurately the temperature distributions of the flows at the evaporator and the condenser sides of the HPHE, as well as the velocity fields, pressure drop and the thermal performance in general of the unit.

Table 6
Investment evaluation.

Installation Main Data		
Total Investment	£	40,000
Power Recovered & Used	kW	100
Additional Power Savings	kW	15
Working Hours per Year	h	8760
Investment Evaluation		
Simple Payback Period	16 Months	

Table 7
Uncertainty associated with instruments used to measure the experimental data.

Parameter	Sensor	Uncertainty
Temperature	NI PXIe-4353	0.05% ± 0.38 °C
Air velocity	Pitot tube type L + manometer	±5% of reading
Flue gas velocity	Pitot tube type L + manometer	±5% of reading
Flue gas pressure	Omega PX1009	±0.25% of reading

In particular, the temperature and the velocity fields across the system should be as uniform as possible in order to enhance the heat recovery in the unit.

The numerical results mentioned are in good agreement with the experimental results. Indeed, it can be noticed that the waste heat recovery measured is 99.5 kW under steady state condition while the numerical thermal power recovered is 101 kW; the difference between the experimental and the calculated values is approximately the 1%.

Furthermore, it is observed that the CFD simulation is also able to reproduce the experimental results in terms of temperatures at the outlets of the evaporator and of the condenser.

Therefore, the validation of the numerical model can be considered satisfactory, since the assessment of the accuracy of the computational simulation by comparison with the experimental data is in the range of 1%.

As a consequence, the CFD approach is demonstrated to be a reliable and important tool in the investigation of the thermal performance of the HPHE because it enables a visualisation of the fluid dynamics behaviour that cannot be identified with experiments.

Indeed, the computational fluid dynamic approach highlighted hot and cold spots as well as the flow field distribution in the unit equipped with finned heat pipe tubes.

4.6. Uncertainty associated with the experimental results

The uncertainty associated with the experimental heat recovery results from uncertainty associated with the measurements of temperature and flow rate. The uncertainty associated with the measurements of the temperature is (0.05% reading ± 0.38 °C), while the one associated with the air flow meter is ±5% of the full scale as listed in Table 8. Therefore, the propagation of uncertainty associated with experimental heat recovery can be calculated using Equation (32) according to Taylor [42]:

$$S_Q = Q_{out} \times \sqrt{\left(\frac{S_{\dot{V}}}{\dot{V}}\right)^2 + \left(\frac{S_{(T_{air,out}-T_{air,in})}}{(T_{air,out}-T_{air,in})}\right)^2} \quad (32)$$

where $S_{(T_{air,out}-T_{air,in})}$ is the uncertainty associated with the difference in temperature, and$S_{\dot{V}}$ is the uncertainty associated with the air flow rate. The error associated with temperature difference between the air inlet and outlet is:

$$S_{(T_{air,out}-T_{air,in})} = \sqrt{S^2_{T_{air,out}} + S^2_{T_{air,in}}} \quad (33)$$

As shown in Table 7 the error associated with the temperature measurements is 0.38 °C.

The maximum error associated with the experimental heat transfer rate of the HPHE are shown in Table 8.

5. Conclusion

A HPHE installed to recovery waste heat from a ceramic kiln was investigated experimentally, theoretically, and numerically. The HPHE installed in the plant managed to recover up to 876 MWh per year. The inlet and outlet of the system were constant at a steady state and within the design parameters of the system. Variations occurred during the tests when the kiln was shut or in stand-by mode. It was observed that the response time of the HPHE was fast, as once the flue gas is introduced into the evaporator section, the air outlet increases soon after. The HPHE thermal performance was predicted theoretically, and the predictions were in agreement with the experimental results. The predicted heat recovery was 100.5 kW while the measured heat recovery was 99.5 kW. Moreover, a steady state CFD simulation of the full geometry of a heat pipe heat exchanger has been carried out and the thermal performance of the HPHE has been investigated. The CFD model accounts for the full 3D geometry of the system that includes the evaporator, the condenser, the separation plate and 18 rows of finned heat pipes tubes. The thermal performance of the simulated geometry is estimated by implementing the design parameters as boundary conditions, i.e. temperatures and flow rates of the primary and secondary flows, respectively, in the evaporator and in the condenser. The numerical results demonstrated that it is possible to recover a thermal power of approximately 101 kW in the unit; the

Table 8
Maximum errors associated with the experimental heat transfer rate.

Heat transfer rate,$\boldsymbol{Q_{out}}$ (kW)	Absolute maximum error, $\boldsymbol{S_Q}$(kW)	Maximum relative error $\frac{\boldsymbol{S_Q}}{\boldsymbol{Q_{out}}}$(%)
76	3.81	5.01
80	3.99	5.01
95	4.78	5.01
99	4.97	5.01
100	4.99	5.01

numerical results are finally compared with the experimental data and the error between the experiment under steady state conditions and the calculations was approximately the 1%. The validation of the theoretical model developed in this paper can lead to a replicability tool to be used on an industrial level. As the tool can be easily adapted to the requirements, the design, fabrication and installations processes of HPHE, the developed approach will lead to significant amount of waste heat recovered and lower greenhouse gases emissions. By developing a CFD model, this paper will contribute to the advancement in the management of fouling and fluid dynamics improvement on both the condenser and evaporator section of a HPHE.

Authorship contributions

All persons who meet authorship criteria are listed as authors, and all authors certify that they have participated sufficiently in the work to take public responsibility for the content, including participation in the concept, design, analysis, writing, or revision of the manuscript. Furthermore, each author certifies that this material or similar material has not been and will not be submitted to or published in any other publication before its appearance in the *Energy, the International Journal.*

Please indicate the specific contributions made by each author (list the authors' initials followed by their surnames, e.g., Y.L. Cheung). The name of each author must appear at least once in each of the three categories below.

All the authors contributed to the article equally.

Declaration of competing interest

The authors declare that they have no known competing financial interests or personal relationships that could have appeared to influence the work reported in this paper.

Acknowledgment

The research presented in this paper has received funding from the European Union's Horizon 2020 framework under grant agreement No. 723641 Design for Resource and Energy efficiency in ceramic kilns and from Innovation and Networks Executive Agency (INEA, European Commission under project H2020 ETEKINA (heat pipE TECHnologies for INdustrial Applications) Contact number: 768772.

References

[1] Monfort E, Mezquita A, Granel R, Vaquer E, Escrig A, Miralles Vz A. Analysis of energy consumption and carbon dioxide emissions in ceramic tile manufacture. Bol La Soc Esp Ceram y Vidr 2010;49:303–10.
[2] European Comission. Reference document on best available techniques in the ceramic manufacturing industry 2007:210–1.
[3] Peng J, Zhao Y, Jiao L, Zheng W, Zeng L. CO2 emission calculation and reduction options in ceramic tile manufacture-the foshan case. Energy Procedia 2012;16:467–76. https://doi.org/10.1016/j.egypro.2012.01.076.
[4] Laboratory LLN. U.S. energy use drops in 2008 n.d.
[5] Mezquita Aa, Monfort Ea, Zaera V. Ceramic tiles manufacturing and emisión trading scheme: reduction of CO2 emissions, European benchmarking. Bol La Soc Esp Ceram y Vidr 2009;48:211–22.
[6] Abdelaziz EA, Saidur R, Mekhilef S. A review on energy saving strategies in industrial sector. Renew Sustain Energy Rev 2011;15:150–68. https://doi.org/10.1016/j.rser.2010.09.003.
[7] Agrafiotis C, Tsoutsos T. Energy saving technologies in the European ceramic sector: a systematic review. Appl Therm Eng 2001;21:1231–49. https://doi.org/10.1016/S1359-4311(01)00006-0.
[8] Anonymous. Industrial microwave drying makes the breakthrough 1995;5:230–1.
[9] Peris B, Navarro-Esbrí J, Molés F, Mota-Babiloni A. Experimental study of an ORC (organic Rankine cycle) for low grade waste heat recovery in a ceramic industry. Energy 2015;85:534–42. https://doi.org/10.1016/j.energy.2015.03.065.
[10] Mezquita A, Boix J, Monfort E, Mallol G. Energy saving in ceramic tile kilns: cooling gas heat recovery. Appl Therm Eng 2014;65:102–10. https://doi.org/10.1016/j.applthermaleng.2014.01.002.
[11] Rentz O, Schmittinger A, Jochum R, Schultmann F. Exemplary investigation into the state of practical realisation of integrated environmental protection within the ceramics industry under observance of the IPPC-directive and the development of BAT reference documents, vols. 44–52. French- German Institute for Environ; 2001.
[12] Beltran J. Cogeneration systems in the ceramics tile sector. In: Proceedings of the workshop on new technologies for the rational use of energy in the ceramics tiles industry. Spain: EC: DG for Ene. Castellon de La Plana; 1994.
[13] Jouhara H, Robinson AJ. Experimental investigation of small diameter two-phase closed thermosyphons charged with water, FC-84, FC-77 and FC-3283. Appl Therm Eng 2010;30:201–11. https://doi.org/10.1016/j.applthermaleng.2009.08.007.
[14] Fadhl B, Wrobel LC, Jouhara H. CFD modelling of a two-phase closed thermosyphon charged with R134a and R404a. Appl Therm Eng 2015;78:482–90. https://doi.org/10.1016/j.applthermaleng.2014.12.062.
[15] Jouhara H, Szulgowska-Zgrzywa M, Sayegh MA, Milko J, Danielewicz J, Nannou TK, et al. The performance of a heat pipe based solar PV/T roof collector and its potential contribution in district heating applications. Energy 2017;136:117–25. https://doi.org/10.1016/j.energy.2016.04.070.
[16] Jouhara H, Serey N, Khordehgah N, Bennett R, Almahmoud S, Lester SP. Investigation, development and experimental analyses of a heat pipe based battery thermal management system. Int J Thermofluids 2020;1–2:100004. https://doi.org/10.1016/j.ijft.2019.100004.
[17] Egilegor B, Jouhara H, Zuazua J, Al-Mansour F, Plesnik K, Montorsi L, et al. ETEKINA: analysis of the potential for waste heat recovery in three sectors: aluminium low pressure die casting, steel sector and ceramic tiles manufacturing sector. Int J Thermofluids 2020;1–2:100002. https://doi.org/10.1016/j.ijft.2019.100002.
[18] Brough D, Mezquita A, Ferrer S, Segarra C, Chauhan A, Almahmoud S, et al. An experimental study and computational validation of waste heat recovery from a lab scale ceramic kiln using a vertical multi-pass heat pipe heat exchanger. Energy 2020;208:118325. https://doi.org/10.1016/j.energy.2020.118325.
[19] Lukitobudi AR, Akbarzadeh A, Johnson PW, Hendy P. Design, construction and testing of a thermosyphon heat exchanger for medium temperature heat recovery in bakeries. Heat Recovery Syst CHP 1995;15:481–91. https://doi.org/10.1016/0890-4332(95)90057-8.
[20] Yang F, Yuan X, Lin G. Waste heat recovery using heat pipe heat exchanger for heating automobile using exhaust gas. Appl Therm Eng 2003;23:367–72. https://doi.org/10.1016/S1359-4311(02)00190-4.
[21] Ramos J, Chong A, Jouhara H. Experimental and numerical investigation of a cross flow air-to-water heat pipe-based heat exchanger used in waste heat recovery. Int J Heat Mass Tran 2016;102:1267–81. https://doi.org/10.1016/j.ijheatmasstransfer.2016.06.100.
[22] Jouhara H, Meskimmon R. Heat pipe based thermal management systems for energy-efficient data centres. Energy 2014;77:265–70. https://doi.org/10.1016/j.energy.2014.08.085.
[23] Almahmoud S, Jouhara H. Experimental and theoretical investigation on a radiative flat heat pipe heat exchanger. Energy 2019;174:972–84. https://doi.org/10.1016/j.energy.2019.03.027.
[24] Delpech B, Axcell B, Jouhara H. Experimental investigation of a radiative heat pipe for waste heat recovery in a ceramics kiln. Energy 2019;170:636–51. https://doi.org/10.1016/j.energy.2018.12.133.
[25] Aslam Bhutta MM, Hayat N, Bashir MH, Khan AR, Ahmad KN, Khan S. CFD applications in various heat exchangers design: a review. Appl Therm Eng 2012;32:1–12. https://doi.org/10.1016/j.applthermaleng.2011.09.001.
[26] Montorsi L, Milani M, Stefani M, Terzi S. Numerical analysis of the exhaust gases recovery from a turbine CHP unit to improve the energy efficiency of a ceramic kiln. Therm Sci Eng Prog 2018;5:444–53. https://doi.org/10.1016/j.tsep.2018.01.013.
[27] Milani M, Montorsi L, Venturelli M, Tiscar JM, García-Ten J. A numerical approach for the combined analysis of the dynamic thermal behaviour of an entire ceramic roller kiln and the stress formation in the tiles. Energy; 2019. https://doi.org/10.1016/j.energy.2019.04.037.
[28] Milani M, Montorsi L, Storchi G, Venturelli M, Angeli D, Leonforte A, et al. Experimental and numerical analysis of a liquid aluminium injector for an Al-H2O based hydrogen production system. Int J Thermofluids 2020. https://doi.org/10.1016/j.ijft.2020.100018. 100018.
[29] Yaïci W, Ghorab M, Entchev E. 3D CFD analysis of the effect of inlet air flow maldistribution on the fluid flow and heat transfer performances of plate-fin-and-tube laminar heat exchangers. Int J Heat Mass Tran 2014;74:490–500. https://doi.org/10.1016/j.ijheatmasstransfer.2014.03.034.
[30] Pal E, Kumar I, Joshi JB, Maheshwari NK. CFD simulations of shell-side flow in a shell-and-tube type heat exchanger with and without baffles. Chem Eng Sci 2016;143:314–40. https://doi.org/10.1016/j.ces.2016.01.011.
[31] Liu C, Bu W, Xu D. Multi-objective shape optimization of a plate-fin heat exchanger using CFD and multi-objective genetic algorithm. Int J Heat Mass Tran 2017;111:65–82. https://doi.org/10.1016/j.ijheatmasstransfer.2017.03.066.
[32] Mroue H, Ramos JB, Wrobel LC, Jouhara H. Experimental and numerical investigation of an air-to-water heat pipe-based heat exchanger. Appl Therm Eng 2015;78:339–50. https://doi.org/10.1016/j.applthermaleng.2015.01.005.

[33] Danielewicz J, Śniechowska B, Sayegh MA, Fidorów N, Jouhara H. Three-dimensional numerical model of heat losses from district heating network pre-insulated pipes buried in the ground. Energy 2016;108:172–84. https://doi.org/10.1016/j.energy.2015.07.012.
[34] Milani M, Montorsi L, Terzi S. Numerical analysis of the heat recovery efficiency for the post-combustion flue gas treatment in a coffee roaster plant. Energy 2017;141:729–43. https://doi.org/10.1016/j.energy.2017.09.098.
[35] Delpech B, Milani M, Montorsi L, Boscardin D, Chauhan A, Almahmoud S, et al. Energy efficiency enhancement and waste heat recovery in industrial processes by means of the heat pipe technology: case of the ceramic industry. Energy 2018;158. https://doi.org/10.1016/j.energy.2018.06.041.
[36] Rohsenow Editor WM, Hartnett Editor JR, Cho Editor YI, San NY, Washington F, Auckland DC, et al. Handbook of heat transfer. 1998.
[37] Rohsenow WM. A method of correlating heat transfer data for surface boiling of liquids. Cambridge, Mass: MIT Division of Industrial Cooporation; 1951. p. 1951.
[38] Guichet V, Almahmoud S, Jouhara H. Nucleate pool boiling heat transfer in wickless heat pipes (two-phase closed thermosyphons): a critical review of correlations. Therm Sci Eng Prog 2019;13. https://doi.org/10.1016/j.tsep.2019.100384.
[39] Nusselt W. The condensation of steam on cooled surfaces. Z Ver Dtsch Ing 1916;60:541–6.
[40] Guichet V, Jouhara H. Condensation, evaporation and boiling of falling films in wickless heat pipes (two-phase closed thermosyphons): a critical review of correlations. Int J Thermofluids 2020;1–2:100001. https://doi.org/10.1016/j.ijft.2019.100001.
[41] Stasiulevicius J, Skrinska A. Heat transfer in banks of finned tubes in crossflow. Vilnius, USSR Mintis 1974;243:1066–71.
[42] Yudin VF. Teploobmen poperechno orebrennykh trub. Leningr: Mashinostroenie; 1982.
[43] Kakac S, Shah RK, Aung W. Handbook of single-phase convective heat transfer. United States: John Wiley and Sons Inc; 1987.
[44] Cao E. Heat transfer in process engineering. New York: McGraw-Hill; 2010.
[45] Danielewicz J, Sayegh MA, Śniechowska B, Szulgowska-Zgrzywa M, Jouhara H. Experimental and analytical performance investigation of air to air two phase closed thermosyphon based heat exchangers. Energy 2014;77:82–7. https://doi.org/10.1016/j.energy.2014.04.107.
[46] Holman J. Heat transfer. McGraw-Hill Education; 2009.
[47] Shabgard H, Allen MJ, Sharifi N, Benn SP, Faghri A, Bergman TL. Heat pipe heat exchangers and heat sinks: opportunities, challenges, applications, analysis, and state of the art. Int J Heat Mass Tran 2015;89:138–58. https://doi.org/10.1016/J.IJHEATMASSTRANSFER.2015.05.020.
[48] Bergman TL, Incropera FP, DeWitt DP, Lavine AS. Fundamentals of heat and mass transfer. seventh ed. USA: John Wiley & Sons; 2011.
[49] Menter F. Zonal two equation k-w turbulence models for aerodynamic flows. 23rd fluid dyn. Plasmadynamics, lasers conf. Reston, Virigina: American Institute of Aeronautics and Astronautics; 1993. https://doi.org/10.2514/6.1993-2906.